Journal of Thermal Analysis and Calorimetry (2023) 148:9701–9721
https://doi.org/10.1007/s10973-023-12342-7

A comparative analysis of parabolic trough collector (PTC) using a hybrid nanofluid

Ibtissem Saddouri[1] · Oussama Rejeb[2] · Djaffar Semmar[3] · Abdelmajid Jemni[1]

Received: 10 March 2023 / Accepted: 23 June 2023 / Published online: 7 August 2023

Abstract
Solar energy can be converted into thermal energy that can be utilized in both residential and industrial applications by using a parabolic through collector (PTC). Hybrid nanofluids are innovative heat transfer fluids made up of a base fluid and solid nanometer-sized particles (nanoparticles) that significantly boost the thermal properties of the fluid and, in turn, the system's thermal performance. The working fluid for considered PTC used in this paper is a hybrid nanofluid. This study gives a comprehensive, thorough thermo-mathematical numerical analysis of PTC collectors employing multiwall carbon nanotube-aluminium oxide (MWCNT/Al_2O_3) hybrid nanofluids in a subtropical desert with moderate winters and very hot, sunny summers. A temperature variation in the components of the PTC, thermodynamic (energy, the exergy of the solar collector under hot desert conditions is carried out using an Engineering Equation Solver (EES). The numerical model was initially checked against published experimental data, and a reasonable agreement was achieved. Results reveal that an increase in nanoparticle concentration could positively influence the performance of the PTC collector. When the 1.5% MWCNT/1.5% Al_2O_3-water hybrid nanofluid is regarded as a cooling fluid, the maximum outlet fluid temperature, energy, the exergy of the PTC collector are achieved. The PTC operates effectively on a summer day under hot climatic circumstances while limiting performance on winter days. For the summer day, the maximum energy, the exergy generated by the PTC using a 1.5% MWCNT/1.5% Al_2O_3-water hybrid nanofluid, is 5066 W, and 876 W, respectively.

Keywords Parabolic through collector (PTC) · Hybrid nanofluids · Multiwall carbon nanotube- aluminum oxide (MWCNT/ Al_2O_3) · Energy · Exergy

Introduction

Solar energy is the world's most important and commonly available renewable energy source. Due to its many benefits, including its lack of environmental impact, the potential to last for generations, and high availability, solar power has attracted a lot of interest. Due to the quantity and inexhaustibility of the solar resource, solar thermal collectors and photovoltaic panels are seen as advantageous ways of capturing and turning solar energy into useful energy. This is possible because of the photo-conversion phenomenon occurring in the photovoltaic module, which is converting some of the sun's rays into usable electrical power [1–4]. A solar thermal (ST) collector is useful because it can turn the heat energy from the sun's rays into thermal heat that can be used [5–10]. Both concentrating and non-concentrating methods can be used to transform solar energy into thermal energy. The most common types of concentrating solar systems that may generate high temperatures are the linear Fresnel [11–14], solar

✉ Ibtissem Saddouri
ibtissemsaddouri35@gmail.com

✉ Oussama Rejeb
Orejeb@sharjah.ac.ae

1 Université de Monastir,, Ecole Nationale d'Ingénieurs de Monastir (ENIM), Laboratoire d'Etudes des Systèmes Thermiques et Energétiques (LESTE), LR99ES31, 5000 Monastir, Tunisia

2 Sustinable Energy Development Research Group, Research Institute for Science and Engineering (RISE), University of Sharjah, P.O. Box 27272, Sharjah, United Arab Emirates

3 Surface de Treatment and Materials Laboratory, Department of Renewable Energy, Faculty of Technology, University of Blida 1, Soumâa Street No. 270, 09000 Blida, Algeria

power tower, dish [15, 16], and parabolic trough collectors. With its technological maturity and economic competitiveness, parabolic trough collector (PTC) technology [17–21] has been tested and evaluated in many power production stations worldwide [22–31]. Direct solar radiation heats the working fluid in a PTSC system. The collector's efficiency improves when the enclosure is comprised of glass, and convection losses are reduced. This system uses the heat from the sun on the receiver to increase the intensity of the sunlight. PTCs can be employed in temperatures ranging from 50 to 400 degrees Celsius, which corresponds to the operating temperature range of the working fluid. [32] Under the climatic circumstances of Tunis, Tunisia (Latitude 36°50′ N and Longitude 10°44′ E), Chafie el al. [33] conducted an experimental analysis to estimate the thermal performance of a PTC. As a cooling medium, Transcal N. Oil was used. Based on their findings, the average energy efficiency for cloudy and sunny days was 19.72% and 8.51%, respectively. Numerous studies have been conducted to enhance PTCs' thermal and optical performance because of their substantial benefits. Using vegetable oils [34], molten salts [35, 36], and nanofluid [37–42] as a cooling fluid improves the physical properties of the heat transfer fluid (HTF), which in turn improves the thermal performance of PTC. On the other hand, inserts, tabulators, a wavy shape, or corrugated tubes [43–45] have been considered for their potential to alter the heat transfer exchange and hence the collectors' efficiency. Xiaowei Zhu el al. [46] proposed a wavy-tape insert for the parabolic trough collector to boost performance by increasing heat transmission within the absorber tube. Their findings show that the total entropy generation rate inside the absorber tube is reduced by between 30.2% and 81.8%. Jaramilloel al. [47] suggested enhancing heat in the receiver tube by incorporating a twisted tape. They developed a thermodynamic model that can be used to evaluate the efficiency of a parabolic trough collector equipped with a twisted tape insert. They found that the Nusselt number, removal factor, friction factor, and thermal efficiency could be improved when a twisted tape insert was inserted. Yilmaz el al. [48]conducted numerical research into the feasibility of using wall-detached twisted tape to improve heat transfer in a parabolic trough receiver. Their research demonstrates a considerable improvement in heat transfer performance, a reduction in a circumferential temperature difference (up to 68%), and an increase in thermal efficiency (up to 10%) compared to a receiver with a simple absorber tube.

Nanoparticles dispersed in a base fluid such as water or oil can improve heat transfer inside the PTC. Scientists have been intrigued by colloidal suspensions of nano-sized particles in a liquid media. In contrast with conventional heat transfer fluids, nanofluids have excellent thermal conductivities and heat transfer coefficients. Because solids have higher thermal conductivity values than liquids, adding solid nanoparticles to a fluid can result in a suspension with superior thermophysical properties. Incorporating nanofluids in PTC decreases thermal resistance by convection between the fluid and the tube, resulting in increased thermal productivity. PTC's thermal improvement using nanofluid is analyzed by Hachicha el al. [49]. Results show that increasing the MWCNTs nanoparticle concentration from 0.05% to 0.1% and then to 0.3% increases the annual average Nusselt number by 12%, 16%, and 21%, respectively, compared to conventional fluid. Bellos et al. [50] developed a thermal analysis to evaluate the performance of PTC using CuO and Al_2O_3 nanoparticles in synthetic oil transfer heat. According to their research, using nanofluids in PTC increased heat transfer enhancement by 50%, with CuO nanofluid performing better than Al_2O_3 nanofluid. However, at a high concentration ratio and a low mass flow rate of nanofluid, CuO and Al_2O_3 showed a 1.26% and 1.13% improvement in PTC thermal efficiency, respectively. Under Tehran's weather circumstances, energy and exergy evaluations of a parabolic trough solar collector (PTC) with Al_2O_3/water and CuO/water as the cooling fluid were conducted by Ehyaei el al.[51]. Their research concluded that the annual average exergy efficiency could be improved by 1.98% and 0.93% when using Al_2O_3/water and CuO/water as cooling fluids, respectively.

There appears to be a significant lack of literature on the PTC behavior when a hybrid nanofluid is used as the cooling fluid. Furthermore, hybrid nanofluid is more feasible than carbon nanotubes since it is cheaper and has better thermal conductivity than nanofluids made from metal oxides. However, there is no research published in the literature on using a multiwall carbon nanotube-aluminum oxide (MWCNT/Al_2O_3) as a heat transfer in a PTC collector. On other hand. Furthermore, for the first time, this study gives a complete comprehensive numerical study on PTC collectors employing multiwall carbon nanotube-aluminum oxide (MWCNT/Al_2O_3) hybrid nanofluids in a subtropical desert with moderate winters and very hot, sunny summers. The following is the outline of the investigation: Section "System description" explains the PTC collector's design. We introduce the PTC mathematical model using a hybrid nanofluid in Section "Thermodynamic modeling". Section "Performance criteria" discusses the PTC's effectiveness in a subtropical desert environment. Finally, the study's concluding conclusions are presented in Section "Results and discussion".

System description

Figure 1 shows a schematic diagram of a parabolic trough collector (PTC). It is made up of a reflector, a glass envelope, an absorber pipe, and a working fluid. The mirrors (reflector) were designed on parabola shape to convert and concentrated radiation rays on the absorber received.

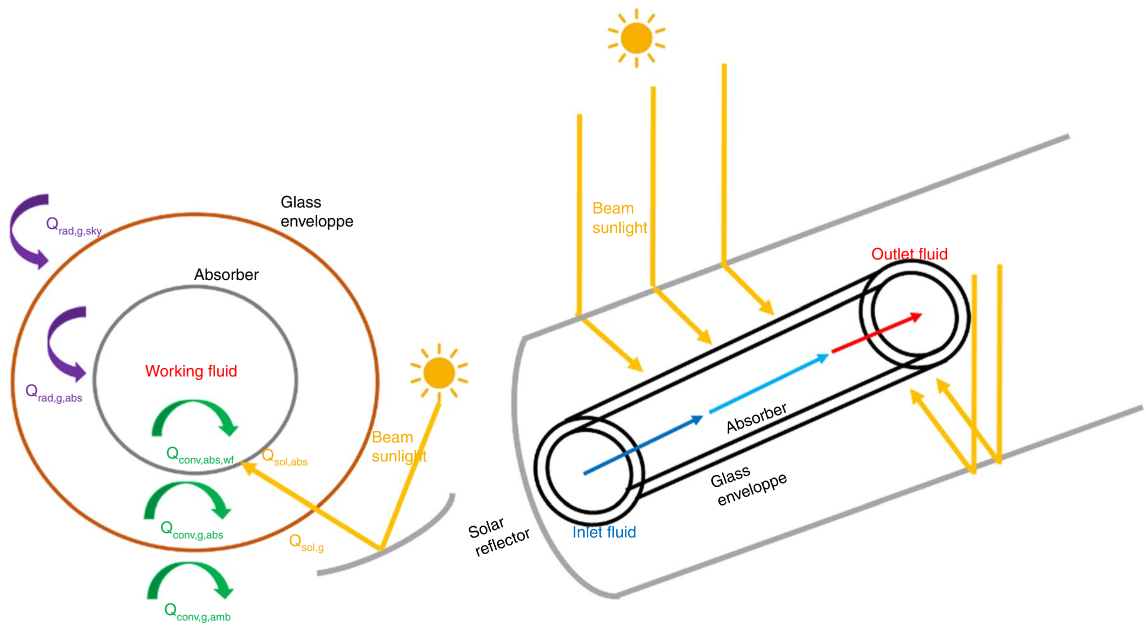

Fig. 1 Schematic diagram of the Solar PTC system

Table 1 summarizes the key properties of this PTC collector. The PTC's solar flux is reflected on the reflector and then passes through the glass envelope to reach the absorber. The absorber is a tube which has a selective coating applied to it to increase its absorptivity and reduce thermal losses. The absorber distributes its heat to the cooling fluid circulating

Table 1 Design conditions of the proposed system

Units	Parameter	Value	Unit
PTC	Width of the PTC	12.27	m
	Length of the PTC	5.76	m
	Diameter of inner of the glazing	0.115	m
	Diameter of outer of the glazing	0.121	m
	Diameter of inner of the pipe	0.066	m
	Diameter of outer of the pipe	0.07	m
	Reflectance of mirror	0.94	–
Nanoparticle	Density of the Al_2O_3 nanoparticle	3970	Kg m^{-3}
	Thermal conductivity of Al_2O_3 nanoparticle	40	W/m^{-1} K^{-1}
	Specific heat capacity of Al_2O_3 nanoparticle	765	J/Kg^{-1} K^{-1}
	Density of the MWCNT nanoparticle	1600	Kg m^{-3}
	Thermal conductivity of MWCNT nanoparticle	3000	W/m^{-1} K^{-1}
	Specific heat capacity of MWCNT nanoparticle	769	J/Kg^{-1} K^{-1}
Base fluid (water)	Density of the base fluid (water) with the temperature is given in (°C)	$\rho_{bf} = 1046.31 - 0.275328T_{wf} - 0,00186353T_{wf}^2$	Kg m^{-3}
	Thermal conductivity of the base fluid (water) with the temperature is given in (°C)	$K_w = 0.616523 + 0.00171586T_{wf} - 0,000005750035T_{wf}^2$	W/m^{-1} °C^{-1}
	Viscosity of the base fluid (water) with the temperature is given in in (°C)	$\mu_w = 0,00161596 - 0,0000420691\ T_{wf} + 6,41265.10^{-7} \cdot\ T_{wf}^2$ $-5,21218.10^{-9} \cdot\ T_{wf}^3 + 1,69963.10^{-11} \cdot\ T_{wf}^4$	Kg/ms
	Specific heat of the base fluid (water) with the temperature is given in in (°C)	$Cp_w = 3906,63 + 3,94005T_{wf} - 0,059366 \cdot\ T_{wf}^2$ $+0,000473391 \cdot\ T_{wf}^3 - 0,00000143726 \cdot\ T_{wf}^4$	J/Kg^{-1} °C^{-1}

inside the tube via convection and then heats it. The fluid's exit temperature is significantly larger than its inlet temperature. In addition, the annular space between the absorber and the glass envelope is vacuumed to reduce heat loss. As a result, the natural convection and radiation heat transfer exchanges between the glazing and the absorber pipe are considered. Multiwall carbon nanotube/aluminum oxide (MWCNT/ Al_2O_3) hybrid nanoparticles [52] are considered in our paper (Table 1). The deionized fluid is water. Using a hybrid nanofluid as a cooling fluid is beneficial because it increases the fluid's thermal conductivity, decreasing the thermal resistance by convection between the tube and the fluid. In our numerical investigation, we chose the Al_2O_3-MWCNT/water hybrid nanofluid. The hybrid nanofluid in this work is considered to be a homogenous mixture of water and Al_2O_3-MWCNT nanoparticles, and the water and the nanoparticles are in thermal equilibrium and at the same flow velocity. No sedimentation and perfectly stable suspension between the nanoparticles and the base fluid are considered in our theoretical mathematical model (Fig. 2).

Thermodynamic modeling

PTC's mathematical model is made up of three heat energy balance equations: the glass envelope, the absorber pipe, and the working fluid [53–58]

For this research, the following assumptions are made:

- On the absorber tube, the distribution of solar flux is homogenous.
- The fluid is incompressible and has a unidirectional flow.

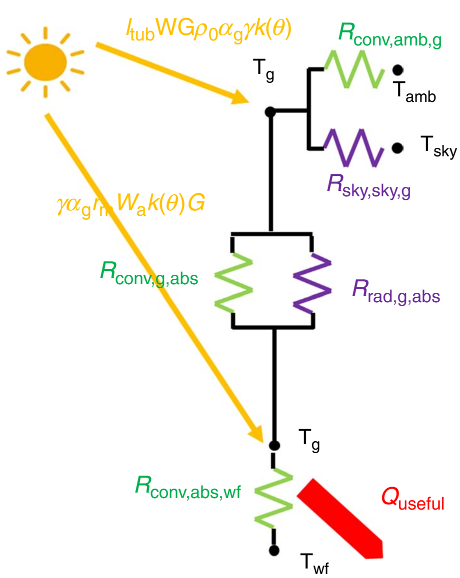

Fig. 2 Schematic diagram of the Solar PTC collector

- Conduction heat in the glazing and absorber pipe is ignored.
- The sky is regarded as a gray body.
- Thermal diffusion is negligible in the glass envelope and tube.
- There is no accumulated dust on the receiver's envelope.
- The incident angle is considered equal to zero (Full tracking).
- Along with the collector, the external and interior convective and radiative exchange coefficients are assumed to be constant.

Glazing envelope

The glass cover loses its heat through convection to the environment $\left(Q_{conv,g\to amb}\right)$ and radiation to the sky $\left(Q_{rad,g\to sky}\right)$, while it absorbs heat from the solar radiation through the reflecting mirror $(l_{tub}WG\rho_0\alpha_g\gamma k(\theta))$ and exchanges the heat by natural convection $(Q_{conv,abs\to g})$ and radiation $(Q_{rad,abs\to g})$ with the absorber pipe.

An energy equation for glazing envelope can be expressed as:

$$0 = l_{tub}WG\rho_0\alpha_g\gamma k(\theta) + Q_{conv,abs\to g} + Q_{rad,abs\to g} - Q_{conv,g\to amb} - Q_{rad,g\to sky} \quad (1)$$

$$0 = Q_{sol,g} + Q_{conv,abs\to g} + Q_{rad,abs\to g} - Q_{conv,g\to amb} - Q_{rad,g\to sky}$$

The amount of solar radiation absorbed by the receiver glass envelope is proportional to the receiver's length (l_{tub}), width (W), intercept factor (γ), reflectance of the reflector (ρ_0), and incidence angle modifier ($k(\theta)$), and the following equation can be used to calculate it:

$$Q_{sol,g} = l_{tub}WG\rho_0\alpha_g\gamma k(\theta) \quad (2)$$

The incidence angle modifier ($k(\theta)$) is estimated by the empirical correlation:

$$k(\theta) = 1 - \left(2.2307 * 10^{-4}\theta\right) - \left(1.1 * 10^{-4}\theta^2\right) + \left(3.18596 * 10^{-6}\theta^3\right) - \left(4.85509 * 10^{-8}\theta^4\right) \quad (3)$$

To simply the calculation, the incident angle equal to zero is considered, and the incidence angle modifier ($k(\theta)$) is equal to 1 (full tracking).

Assuming the sky is a black body with a temperature of T_{sky}, the infrared radiation heat exchanger transfer $\left(Q_{rad,g\to sky}\right)$ from the PTC collector to the the sky can be determined as follows:

$$Q_{rad,g\to sky} = l_{tub}\pi D_{g,ext}\varepsilon_g\sigma(T_g^2 + T_{sky}^2)(T_g + T_{sky})\left(T_g - T_{sky}\right) \quad (4)$$

The convective heat transfer flux ($Q_{conv,g\to amb}$) from the PTC collector to the surroundings used in this work is an empirical correlation depending directly on the velocity of the wind speed (V_{wind}) and the diameter of the glass envelope ($D_{\text{g,ext}}$)

$$Q_{\text{conv,g}\to\text{amb}} = l_{\text{tub}}\pi D_{g,\text{ext}}\left(4V_{\text{wind}}^{0.58})(D_{\text{g,ext}}^{-0.42})\left(T_{\text{g}} - T_{\text{amb}}\right) \quad (5)$$

The free-molecular convection heat exchanges transfer $Q_{\text{conv,abs}\to\text{g}}$ from the absorber pipe to the the glass envelope is proportional to the effective thermal conductivity of the annulus gas (k_{eff}), the outer diameter $\left(D_{\text{ab, out}}\right)$ of the absorber pipe, and the following equation can be used to calculate it:

$$Q_{\text{conv,abs}\to\text{g}} = l_{\text{tub}}\pi D_{\text{abs,ext}}\left(\frac{2k_{\text{eff}}}{D_{\text{abs,ext}}\ln\left(\frac{D_{\text{g,int}}}{D_{\text{abs,ext}}}\right)}\right)(T_{\text{abs}} - T_{\text{g}}) \quad (6)$$

The infrared radiation heat exchanges transfer $Q_{\text{rad,abs}\to\text{g}}$ can be calculate as:

$$Q_{\text{rad,abs}\to\text{g}} = l_{\text{tub}}\pi D_{\text{abs, ext}}\frac{\sigma\left(\left(T_{\text{abs}}^2\right) + (T_{\text{g}}^2)\right)\left(T_{\text{abs}} + T_{\text{g}}\right)}{\frac{1}{\varepsilon_{\text{ab}}} + \frac{1-\varepsilon_{\text{g}}}{\varepsilon_{\text{g}}}\left(\frac{D_{\text{abs, ext}}}{D_{\text{g, int}}}\right)}(T_{\text{abs}} - T_{\text{g}}) \quad (7)$$

Replacing the heat flux exchanges by their expression Eq. (1) becomes

$$\begin{aligned} 0 =& l_{\text{tub}}\pi D_{\text{abs,ext}}\left(\frac{2k_{\text{eff}}}{D_{\text{abs,ext}}\ln\left(\frac{D_{\text{g,int}}}{D_{\text{abs,o}}}\right)}\right)(T_{\text{abs}} - T_{\text{g}}) \\ &+ l_{\text{tub}}\gamma\alpha_{\text{g}}r_{\text{m}}W_{\text{a}}Gk(\theta) + l_{\text{tub}}\pi D_{\text{g, ext}}\varepsilon_{\text{g}}\sigma\left(T_{\text{sky}} - T_{\text{g}}\right) \\ &+ l_{\text{tub}}\pi D_{\text{g,ext}}(D_{\text{g,ext}}^{-0.42})4V_{\text{wind}}^{0.58}\left(T_{\text{amb}} - T_{\text{g}}\right) \\ &+ l_{\text{tub}}\pi D_{\text{ab,ext}}\frac{\sigma\left(\left(T_{\text{ab}}^2\right) + (T_{\text{g}}^2)\right)\left(T_{\text{ab}} + T_{\text{g}}\right)}{\frac{1}{\varepsilon_{\text{ab}}} + \frac{1-\varepsilon_{\text{g}}}{\varepsilon_{\text{g}}}\left(\frac{D_{\text{ab, ext}}}{D_{\text{g, int}}}\right)}\left(T_{\text{abs}} - T_{\text{g}}\right) \end{aligned} \quad (8)$$

Absorber pipe

The absorber pipe absorbs heat from the beam solar radiation attenuated ($\rho_0 l_{\text{tub}}\gamma\alpha_{\text{abs}}\tau_{\text{g}}WGk(\theta)$), exchanges the heat by free-molecular convection ($Q_{\text{conv,abs}\to\text{g}}$ and radiation ($Q_{\text{rad,abs}\to\text{g}}$ with the glass and by convection with the working fluid ($Q_{\text{conv,abs}\to\text{wf}}$.

An energy equation for glazing envelope can be expressed as:

$$0 = Q_{\text{sol,abs}} - Q_{\text{conv,abs}\to\text{g}} - Q_{\text{rad,abs}\to\text{g}} - Q_{\text{conv,abs}\to\text{wf}} \quad (9)$$

The amount of solar radiation absorbed by the receiver pipe is estimated as:

$$Q_{\text{sol,ab}} = \rho_0 l_{\text{tub}}\gamma\alpha_{\text{abs}}\tau_{\text{g}}WGk(\theta) \quad (10)$$

The following equation describes the convection heat transfer from the absorber to the working fluid in accordance with Newton's law:

$$Q_{\text{conv,abs}\to\text{wf}} = l_{\text{tub}}\pi D_{\text{abs,int}}h_{\text{conv, abs}\to\text{wf}}\left(T_{\text{abs}} - T_{\text{wf}}\right) \quad (11)$$

Replacing the heat flux exchanges by their expression Eq. (9) becomes

$$\begin{aligned} 0 =& \rho_0 l_{\text{tub}}\gamma\alpha_{\text{abs}}\tau_{\text{g}}WGk(\theta) + \pi D_{\text{abs, in}}h_{\text{conv, abs}\to\text{wf}}\left(T_{\text{wf}} - T_{\text{abs}}\right) \\ &+ l_{\text{tub}}\pi D_{\text{abs,ext}}\left(\frac{2k_{\text{eff}}}{D_{abs,ext}\ln\left(\frac{D_{\text{g,int}}}{D_{\text{abs,o}}}\right)}\right)(T_{\text{g}} - T_{\text{abs}}) \\ &+ l_{\text{tub}}\pi D_{\text{abs, ext}}\frac{\sigma\left(\left(T_{\text{abs}}^2\right) + (T_{\text{g}}^2)\right)(T_{\text{abs}} + T_{\text{g}})}{\frac{1}{\varepsilon_{\text{abs}}} + \frac{1-\varepsilon_{\text{g}}}{\varepsilon_{\text{g}}}\left(\frac{D_{\text{ab,ext}}}{D_{\text{g,int}}}\right)}\left(T_{\text{g}} - T_{\text{abs}}\right) \end{aligned} \quad (12)$$

Working fluid

The following equation describes the heat balance of the working fluid that flows through the absorber pipe.

$$\dot{m}C_{\text{f}}\Delta T_{\text{f}} = l_{\text{tub}}\pi D_{\text{abs,in}}h_{\text{conv, abs, wf}}\left(T_{\text{abs}} - T_{\text{wf}}\right) \quad (13)$$

As a function of the Nusselt number, the fluid's thermal conductivity, and the tube's hydraulic diameter, the heat transfer coefficient by convection is calculated as:

$$h_{\text{conv,abs,wf}} = \text{Nusselt}_{\text{wf}}\frac{K_{\text{wf}}}{D_{\text{a}}} \quad (14)$$

As a function of the Reynolds and the Prandtl number, the Nusselt number is estimated by the following correlation

$$\text{Nusselt}_{\text{wf}} = 4.364 \quad \text{Re}_{\text{wf}} < 2300(\text{laminar flow}) \quad (15)$$

$$\text{Nusselt}_{\text{wf}} = 0.023 * \left(\text{Re}_{\text{wf}}\right)^{0.8}\left(\text{Pr}_{\text{wf}}\right)^{0.4} \quad 2300 < \text{Re}_{\text{wf}}(\text{Turbulent flow}) \quad (16)$$

It is the ratios of momentum diffusivity to thermal diffusivity that is known as the Prandtl Number, and it estimated as:

$$Pr_{\text{wf}} = \frac{C_{\text{wf}}\mu_{\text{wf}}}{k_{\text{wf}}} \quad (17)$$

The Reynolds number denotes the ratios of inertial forces to viscosity forces, and its calculated as:

$$\mathrm{Re}_{\mathrm{wf}} = \frac{D_{\mathrm{abs,in}}\rho_{\mathrm{wf}}v_{\mathrm{wf}}}{\mu_{\mathrm{wf}}} \tag{18}$$

The following equation is applied to compute the working fluid's velocity:

$$v_{\mathrm{wf}} = \frac{m_{\mathrm{wf}}}{\frac{\pi}{4}D^2_{\mathrm{abs,in}}\rho_{\mathrm{wf}}} \tag{19}$$

For this research, we utilized water as the base fluid. The thermophysical properties of water, which vary with temperature, are employed. Predictions of water's thermophysical properties as a function of temperature can be obtained using the following empirical formulae presented in Table 1.

One of the most crucial thermophysical properties of a working fluid in a thermal system is its thermal conductivity 69–72. The effectiveness of a thermal system can be improved by using a working fluid with a greater thermal conductivity value. The ability of a material to transfer heat is quantified by its thermal conductivity. A function of particle volume fraction, the thermal conductivity particle shape of used two nanoparticles, and the base fluid can be formulated to describe the thermal conductivity of hybrid nanofluids [59–65]. The following equation used in our study, which is based on the modified Maxwell model for hybrid nanofluids, provides an approximate approximation of the thermal conductivity of the hybrid nanofluid:

$$k_{\mathrm{hnf}} = k_{\mathrm{bf}}\frac{\frac{\varphi_{\mathrm{np1}}k_{\mathrm{np1}}+\varphi_{\mathrm{np2}}k_{\mathrm{np2}}}{\varphi_{\mathrm{hnf}}} + 2k_{\mathrm{bf}} + 2\left(\varphi_{\mathrm{np1}}k_{\mathrm{np1}} + \varphi_{\mathrm{np2}}k_{\mathrm{np2}}\right) - 2\varphi_{\mathrm{hnf}}k_{\mathrm{bf}}}{\frac{\varphi_{\mathrm{np1}}k_{\mathrm{np1}}+\varphi_{\mathrm{np2}}k_{\mathrm{np2}}}{\varphi_{\mathrm{hnf}}} + 2k_{\mathrm{bf}} - 2\left(\varphi_{\mathrm{np1}}k_{\mathrm{np1}} + \varphi_{\mathrm{np2}}k_{\mathrm{np2}}\right) + \varphi_{\mathrm{hnf}}k_{\mathrm{bf}}} \tag{20}$$

Density is a crucial factor in thermodynamics. Density significantly impacts the flow Reynolds number, pressure, and heat transfer capability of a hybrid nanofluid. The density of a hybrid nanofluid can be described as a function of the volume fraction, density, shape of the particles of the two nanoparticles utilized, and base fluid density [61–68]. Our work used a hybrid nanofluid, the density of which can be approximately calculated using the following equation, which is based on the modified Pak and Cho correlation:

$$\rho_{\mathrm{hnf}} = \left(1 - \varphi_{\mathrm{hnf}}\right)\rho_{\mathrm{bf}} + \varphi_{\mathrm{np1}}\rho_{\mathrm{np1}} + \varphi_{\mathrm{np2}}\rho_{\mathrm{np2}} \tag{21}$$

Because of frictional effects, the viscosity of hybrid nanofluids is crucial in determining the needed pumping power. The viscosity of a hybrid nanofluid can be described as a function of the volume fraction, density, shape of the particles of the two nanoparticles utilized, and base fluid density [61–68]. The following equation, based on the modified Brinkman correlation for hybrid nanofluids, provides an approximation of the viscosity of the hybrid nanofluid employed in our study:

$$\mu_{\mathrm{nf}} = \frac{\mu_{\mathrm{bf}}}{\left(1 - \varphi_{\mathrm{np1}} - \varphi_{\mathrm{np2}}\right)^{2.5}} \tag{22}$$

Performance criteria

Energy analysis

In order to calculate the PTC's effective gain output, we utilize the following formula.

$$Q_{\mathrm{useful}} = \dot{m}C_{\mathrm{f}}\Delta T_{\mathrm{f}} \tag{23}$$

PTC thermal efficiency is defined as the ratio of useful energy produced to solar energy collected by the PTC and it can be calculated as follows:

$$\eta_{\mathrm{energy,\,PTC}} = Q_{\mathrm{useful}}/Q_{\mathrm{sol,abs}} = \dot{m}C_{\mathrm{f}}\Delta T_{\mathrm{f}}/\rho_0 l_{\mathrm{tub}}\gamma\alpha_{\mathrm{abs}}\tau_{\mathrm{g}}WGk(\theta) \tag{24}$$

Exergy analysis

It is possible that the first law technique cannot yield an in-depth understanding of the system (energy analysis). The system's performance can be quantified and standardized using second-law energy efficiency. Exergy is an useful technique in thermodynamics for achieving irreversibility in a system. The heat transfer irreversibilities between the sun and the collector, the collector and the surrounding air, and within the collector all impact the quantity of usable energy provided by solar PTC collector. An exergy balance equation explicates what processes are wasteful in a thermodynamic solar collector system and supports engineers for achieving an optimal design, providing path for losses reduction. Exergy is also exchanged across control volumes via matter flows. While mass and energy are always preserved, nonidealities (sometimes called irreversibilities) like friction result in the destruction (or annihilation) of exergy inside a system.

A PTC collector (Fig. 3) system's exergy balance is represented as:

$$\dot{Q}_{\mathrm{exergy,sun}} + \dot{Q}_{\mathrm{mass,in}} = \dot{Q}_{\mathrm{mass,out}} + \dot{Q}_{\mathrm{destruction}} \tag{25}$$

The amount of available solar exergy collected by the PTC collector can be estimated using Petla's law, which is based on the relationship between the sun, ambient

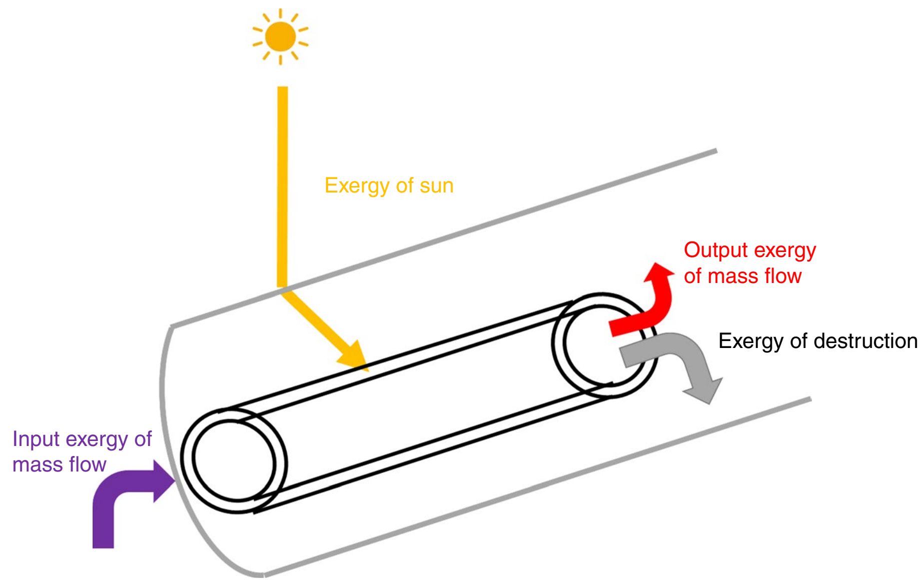

Fig. 3 Schematic exergy flow diagram of the Solar PTC collector

temperatures, and the amount of solar radiation that reach the absorber pipe, and its calculated as:

$$\dot{Q}_{\text{exergy,sun}} = \rho_0 l_{\text{tub}} \gamma \alpha_{\text{abs}} \tau_{\text{g}} WGk(\theta)\left(1 - \frac{4}{3}\frac{T_{\text{amb}}}{T_{\text{sun}}} + \frac{1}{3}\left(\frac{T_{\text{amb}}}{T_{\text{sun}}}\right)^4\right) \quad (26)$$

In order to calculate the output PTC's exergy gain, we utilize the following formula.

$$\dot{Q}_{\text{exergy,th}} = \dot{Q}_{\text{mass,in}} - \dot{Q}_{\text{mass,out}} = \dot{m}_{\text{wf}} C_{\text{f}}\left(T_{\text{out,wf}} - T_{\text{in,wf}}\right) - \dot{m}_{\text{wf}} C_{\text{f}} T_{\text{amb}} \ln\left(\frac{T_{\text{out,wf}}}{T_{\text{in,wf}}}\right) - \dot{m}_{\text{wf}} T_{\text{amb}}\left(\frac{\Delta p}{\rho_{\text{wf}} T_{\text{wf}}}\right) \quad (27)$$

To calculate the pressure drop in the absorber tube, the following equation is used:

$$\Delta p = f \frac{l_{\text{tub}} \rho_{wf}}{D_{\text{abs,in}}} \frac{v_{\text{wf}}^2}{2} \quad (28)$$

The friction factor of the working fluid can be estimated using Petukhov equation, which is based on the Reylonds number, and is calculated as:

$$f = \left(0.79 \ln\left(\text{Re}_{\text{wf}}\right) - 1.64\right)^{-2} \quad (29)$$

PTC exergy efficiency is described as the ratio of usable energy generated to exergy solar energy captured by the PTC, and it can be estimated as:

Results and discussion

Validation

The proposed model is verified by using the results of the experimental investigation conducted by Alfellag [66, 67]. According to their PTC, water serves as the working fluid. Table 1 lists the characteristics of the solar PTC. The current numerical model includes the same solar PTC parameters. Our results are in good accord with experimental results since we employ the same characteristics of the solar PTC in the present computational model (Table 2) (Fig. 4). Our model has proved to be accurate and can be used to assess the performance of solar PTC under various operating circumstances.

Thermophysical properties of hybrid nanofluids

To evaluate the performance of the PTC using hybrid nanofluid as a cooling fluid, it is necessary to understand the effects of nanoparticle concentration and fluid temperature on thermophysical properties (density, specific heat, viscosity, and thermal conductivity) for different hybrid nanofluid concentrations. The basis fluid in this research is water, and its thermophysical parameters, including viscosity, specific heat capacity, thermal conductivity, and density, are acquired via the Engineering Equation Solver (EES) software library. The

$$\eta_{\text{exergy, PTC}} = \dot{Q}_{\text{exergy,th}} / \dot{Q}_{\text{exergy,sun}} = \frac{\dot{m}_{\text{wf}} C_f\left(T_{\text{out,wf}} - T_{\text{in,wf}}\right) - \dot{m}_{\text{wf}} C_f T_{\text{amb}} \ln\left(\frac{T_{\text{out,wf}}}{T_{\text{in,wf}}}\right) - \dot{m}_{\text{wf}} T_{\text{amb}}\left(\frac{\Delta p}{\rho_{\text{wf}} T_{\text{wf}}}\right)}{l_{\text{tub}} \gamma \alpha_{\text{abs}} \rho_0 \tau_{\text{g}}\, WGk(\theta)\left(1 - \frac{4}{3}\frac{T_{\text{amb}}}{T_{\text{sun}}} + \frac{1}{3}\left(\frac{T_{\text{amb}}}{T_{\text{sun}}}\right)^4\right)} \quad (30)$$

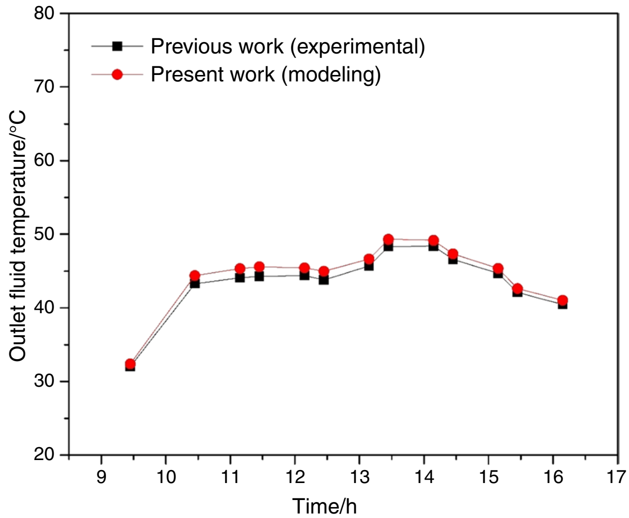

Fig. 4 Comparison between our results and experimental results

thermophysical properties of the working fluid are reduced when the temperature of the operating fluid rises. On the other hand, increased nanoparticle concentration improves thermal conductivity, as seen in Fig. 5.

The convection transfer coefficient is defined by dividing the Nusselt number and the cooling fluid's conductivity by the hydraulic diameter.

The heat transfer coefficient by convection (Fig. 6) was improved by 0.75% when using the mono nanofluid (0.25% MWCNT-water), by 4% when using the hybrid nanofluid (0.25% MWCNT-water and 0.25% Al_2O_3-water), and by 27.1%, when using the hybrid nanofluid (1.5%MWCNT and 1.5% Al_2O_3-water), in comparison with using water as the cooling fluid.

Case study of the proposed system

The proposed PTC is evaluated under "hot desert climate" expressed by Ouarzazate, Morocco (30.55 N, 6.55 W). In addition, comprehensive assessments have been performed on the proposed system in terms of the output fluid temperature, thermal and exergy efficiency, usable heat power, and exergy powers.

According to the Köppen climate classification, Ouarzazate has a hot desert climate (BWh), with warm winters and hot, sunny summers. The average temperature in the coldest month (January) is 9.8 °C, while the average temperature in the warmest month (July) is 30.8 °C. The yearly sun hours are 3416, with the highest monthly sunshine hours of 335 in June and the lowest monthly sunshine hours of 2413 in November.

Figures 7–9 depict the ambient temperature, beam solar radiation, and the wind speed on typical days (January 13, April 30, July 13, and October 7) for each of Ouarzazate's four seasons. Figure 8 displays the beam solar radiation on typical days (January 13, April 30, July 13, and October 7) for each of Ouarzazate's four seasons: The summer has the greatest average temperature (July 13) while the winter has the lowest (January 13). Maximum beam solar radiation irradiation occurs in July at 944.9 W m^{-2}, April 30 at 887.3 W m^{-2}, October 7 at 801.2 W m^{-2}, and January 13 at 582.7 W m^{-2}. Figure 8 depicts the beam solar radiation of days (January 13, April 30, July 13, and October 7) for each of Ouarzazate's four seasons: The summer has the greatest average temperature (July 13) while the winter has the lowest (January 13). Maximum sun irradiation occurs in July at 944.9 W m^{-2}, April 30 at 887.3 W m^{-2}, October 7 at 801.2 W m^{-2}, and January 13 at 582.7 W m^{-2}.

Variations in different components of the PTC

For typical days (January 13, April 30, July 13, and October 7) under Ouarzazate climatic conditions, the transient evolution of the absorber and outlet temperature using water, hybrid nanofluid presented by 0.25% MWCNT/0.25% Al_2O_3-water, and 1.5% MWCNT/1.5% Al_2O_3-water is depicted in Figs. 10, 11.

Figures 10 and 11 show that on a cloudy day (13/01), the PTC's absorber pipe temperature rises from 274.3 K to 372.1 K with water as the cooling fluid, from 274.3 K to 348.9 K with 0.25% MWCNT/0.25% Al_2O_3-water, and from 274.3 K to 345.2 K with 1.5% MWCNT/0.2% Al_2O_3-water. In comparison, the outlet fluid temperature rises from 274.3 K to 323.1 K with water as the cooling fluid, 274.3 K to 323.7 K with 0.25% MWCNT/0.25% Al_2O_3-water, and 274.3 K to 324.6 K with 1.5% MWCNT/1.5% Al_2O_3-water hybrid nanofluid. On a spring day (30/04), when using water as the cooling fluid, the PTC's absorber pipe temperature goes up from 286 to 407.4 K, from 286 to 380.9 K when using a 0.25% MWCNT/0.25% Al_2O_3-water, and from 286 to 376 K when using a 1.5% MWCNT/1.5% Al_2O_3-water. When water is utilized as the cooling fluid, the PTC's output fluid temperature goes up from 286 to 357.2 K, and when 0.25% MWCNT/0.25% Al_2O_3-water hybrid nanofluid is employed, it goes up from 286 K to 358.3 K, and from 286 K to 359.7 K when using a 1.5% MWCNT/1.5% Al_2O_3-water hybrid nanofluid. For a summer day (13/07), the PTC's absorber pipe temperature rises from 296.1 K to 442.9 K with water as the cooling fluid, 296.1 K to 412.9 K with 0.25% MWCNT/0.25% Al_2O_3-water, and 296.1 K to 406.9 K with 1.5% MWCNT/1.5% Al_2O_3-water, while the outlet fluid temperature rises from 296.1 K to 370.6 K with water as the cooling fluid, 296.1 K to 372.1 K with 0.25% MWCNT/0.25% Al_2O_3-water hybrid nanofluid, and 296.1 K to 373.6 K with 1.5% MWCNT/1.5% Al_2O_3-water hybrid nanofluid. On an autumn day (07/10) (30/04), when using water as the cooling fluid, the PTC's

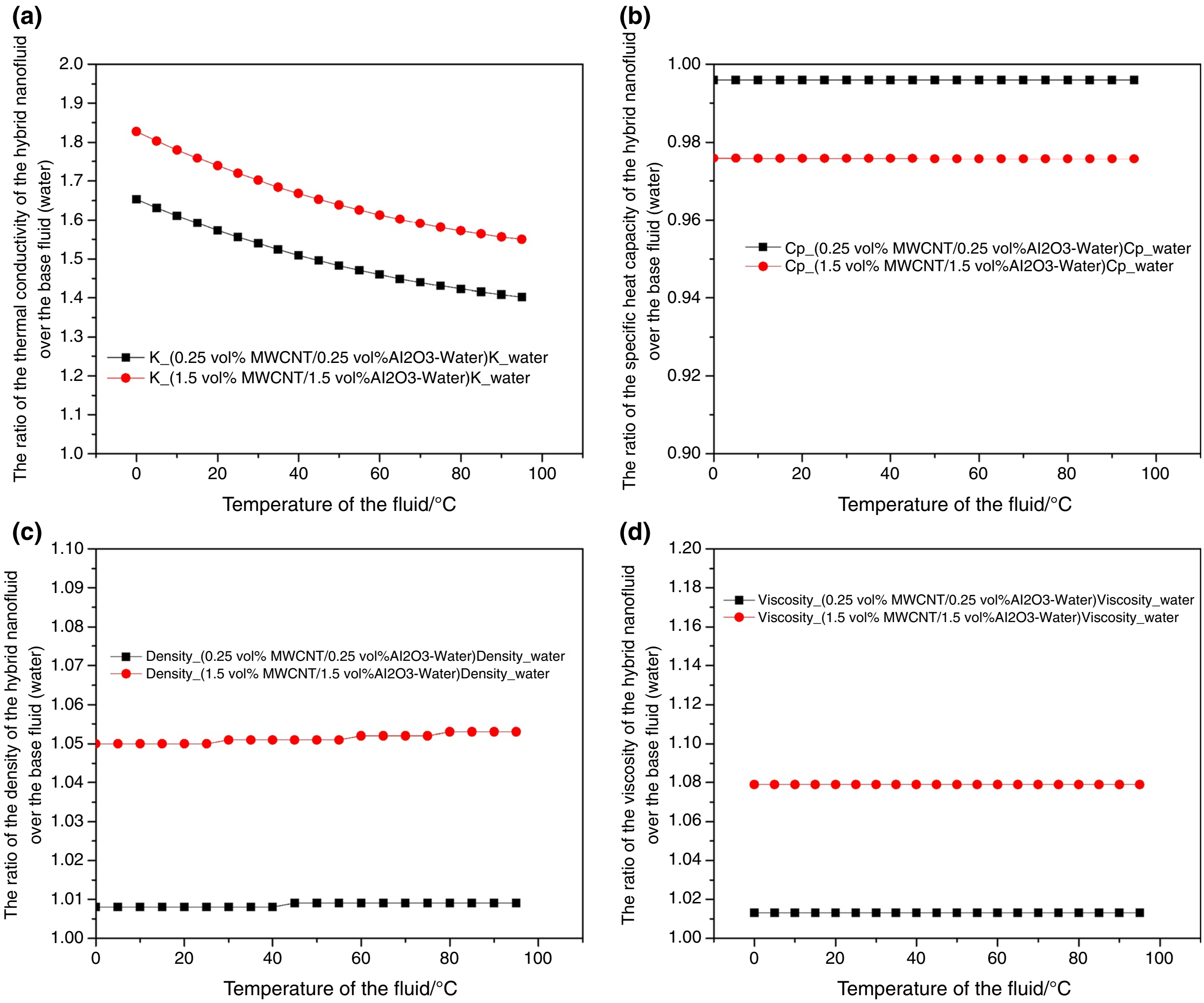

Fig. 5 Thermophysical properties of hybrid nanofluids

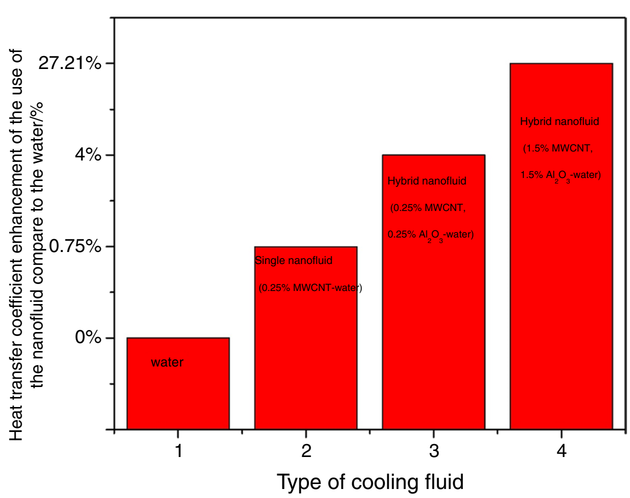

Fig. 6 Heat transfer coefficient enhancement

absorber pipe temperature goes up from 287.6 to 415.9 K, from 287.6 to 388.4 K when using a 0.25% MWCNT/0.25% Al_2O_3-water, and from 287.6 to 382.2 K when using a 0.25% MWCNT/0.25% Al_2O_3-water. When water is utilized as the cooling fluid, the PTC's output fluid temperature goes up from 287.6 to 352.7 K, and when 0.25% MWCNT/0.25% Al_2O_3-water hybrid nanofluid is employed, it goes up from 287.6 to 353.7 K; when using a with 1.5% MWCNT/1.5% Al_2O_3-water hybrid nanofluid, it goes up from 287.6 to 354.9 K.

The evolution of the temperature of all the output fluids, including water, hybrid nanofluid, presented by 0.25% MWCNT/0.2% Al_2O_3-water and 1.5% MWCNT/0.25% Al_2O_3-water is followed by the trend of solar radiation. It peaks in the morning and drops back down to ambient by afternoon. The highest readings are recorded at 1:40 p.m. on January 13, 1:50 p.m. on April 30, 1:30:00 p.m. on July

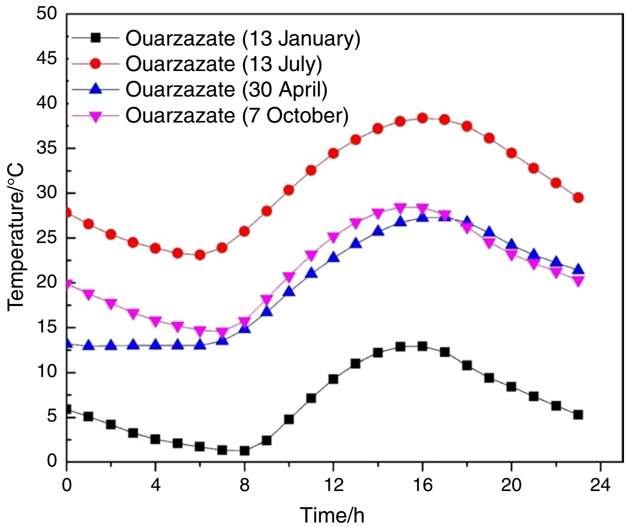

Fig. 7 Ambient temperature on typical days (January 13, April 30, July 13, and October 7)

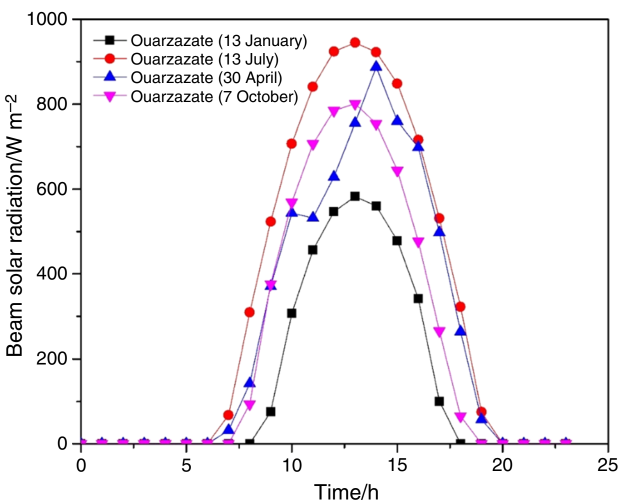

Fig. 8 Beam solar radiation on typical days (January 13, April 30, July 13, and October 7)

14, and 1:40:00 p.m. on October 7. It should be noticed that these times coincide with the peak values of the direct solar radiation absorbed by the solar PTC. When the 1.5% MWCNT/1.5% Al_2O_3-water hybrid-nanofluid is regarded as a cooling fluid, the maximum outlet fluid and the lowest absorber pipe given by PTC are reached for all distinct scenarios of the variation in examined weather conditions. 1.5% MWCNT/1.5% Al_2O_3-water hybrid nanofluid has a higher convective heat transfer coefficient than 0.25%

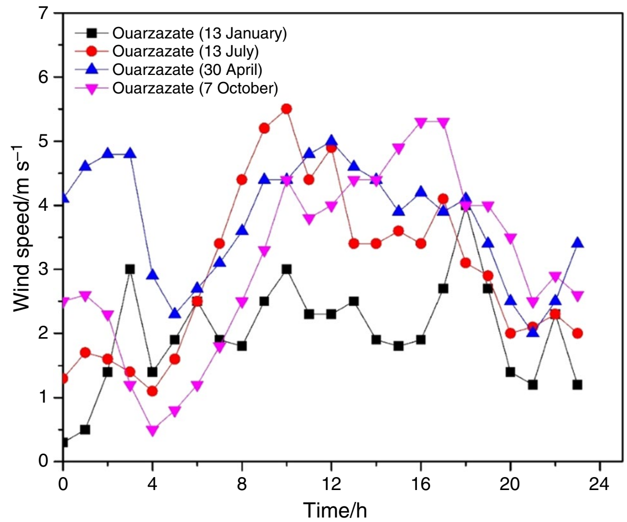

Fig. 9 Wind speed on typical days (January 13, April 30, July 13, and October 7)

MWCNT/0.25% Al_2O_3-water. Increasing the nanoparticles concentration improves the thermal properties of the cooling fluid, such as its thermal conductivity, density, and viscosity. This improves the convective heat transfer between the cooling fluid and the absorber tube wall, which means fewer losses between the absorber pipe and output fluid temperature. Consequently, a smaller temperature gradient (a lower absorber pipe and higher output fluid temperature) is obtained.

Heat useful and exergy power

For typical days (January 13, April 30, July 13, and October 7) under Ouarzazate climatic conditions, the transient evolution of the useful heat and exergy power using water, hybrid nanofluid presented by 0.25% MWCNT/0.25% Al_2O_3-water, and 1.5% MWCNT/1.5% Al_2O_3-water is depicted in Figs. 12, 13. For a chosen cloudy day (13/01) in the Ouarzazate region, the maximum useful heat gain provided by PTC using water, 0.25% MWCNT/0.25% Al_2O_3-water, and 1.5% MWCNT/1.5% Al_2O_3-water hybrid nanofluid as a cooling fluid is 3112 W, 3149W, 3154W, respectively, while the maximum exergy output by PTC using 0.25% MWCNT/0.25% Al_2O_3-water, and 1.5% MWCNT/1.5% Al_2O_3-water hybrid nanofluid as a cooling fluid is 376.3 W, 368.1W, 394.2W, respectively. For a chosen springer day (30/04) in the Ouarzazate region, the maximum useful heat gain provided by PTC using water, 0.25% MWCNT/0.25% Al_2O_3-water, and 1.5% MWCNT/1.5% Al_2O_3-water hybrid nanofluid as a cooling fluid is 4689W, 4760W, and 4772

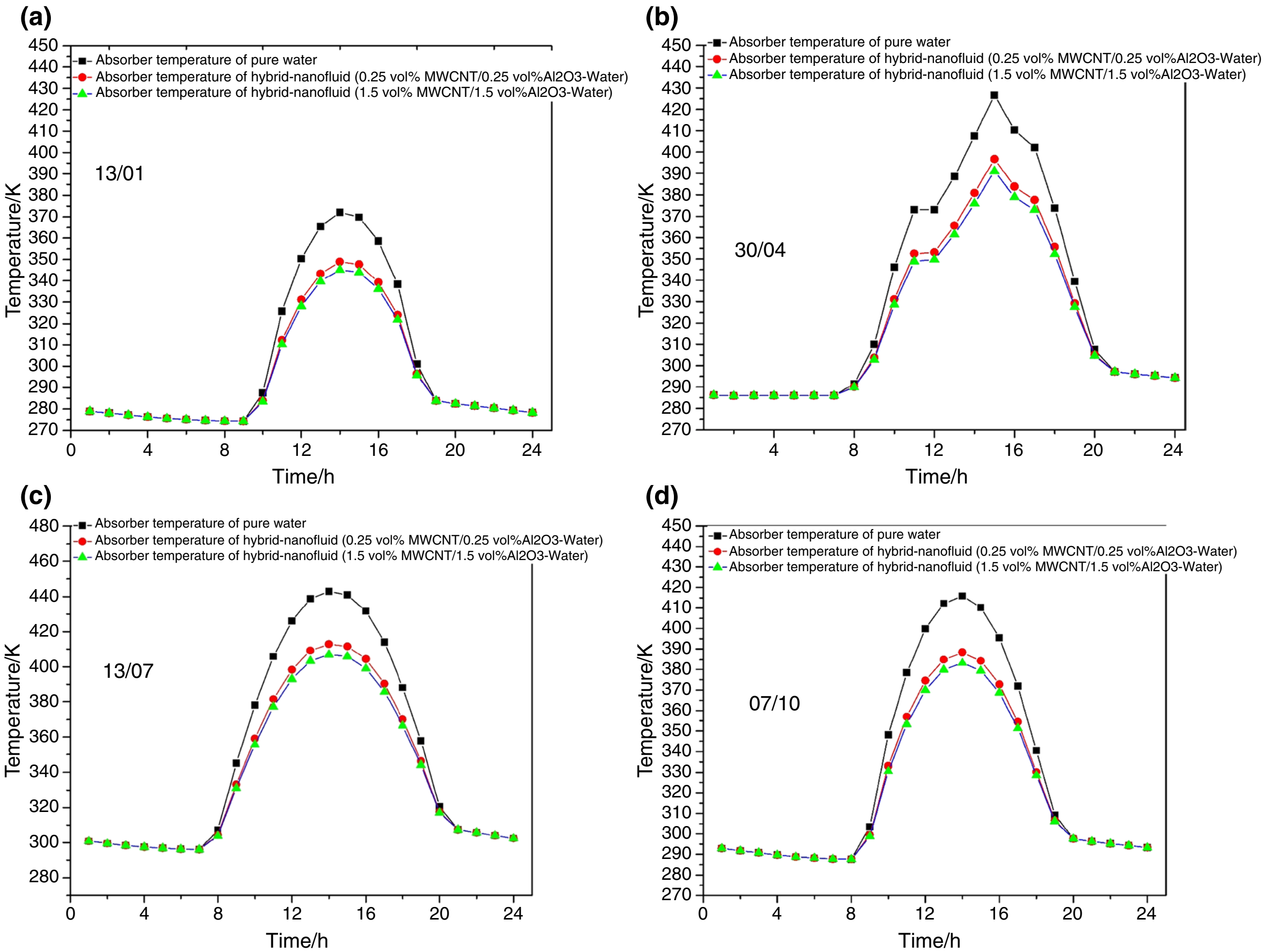

Fig. 10 Absorber pipe temperature for typical days (January 13, April 30, July 13, and October 7) under Ouarzazate climatic conditions

W, respectively, while the maximum exergy output by PTC using water, 0.25% MWCNT/0.25% Al_2O_3-water, and 1.5% MWCNT/1.5% Al_2O_3-water hybrid nanofluid as a cooling fluid is 767.7W, 791.7W, and 808.8 W, respectively. For a chosen summer day (13/07) in the Ouarzazate region, the maximum useful heat gain provided by PTC using water, 0.25% MWCNT/0.25% Al_2O_3-water, and 1.5% MWCNT/1.5% Al_2O_3-water hybrid nanofluid as a cooling fluid is 4973W, 5052W, and 5066 W, respectively, while the maximum exergy output by PTC using water, 0.25% MWCNT/0.25% Al_2O_3-water, and 1.5% MWCNT/1.5% Al_2O_3-water hybrid nanofluid as a cooling fluid is 829.9 W, 857W, 876W, respectively. For a chosen autumn day (07/10) in the Ouarzazate region, the maximum useful heat gain provided by PTC using water, 0.25% CuO/water, 0.25% MWCNT/0.25% Al_2O_3-water, and 1.5% MWCNT/1.5% Al_2O_3-water hybrid nanofluid as a cooling fluid is 4242 W, 4302W, 4312W, respectively, while the maximum exergy output by PTC using water, 0.25% MWCNT/0.25% Al_2O_3-water, and 1.5% MWCNT/1.5% Al_2O_3-water hybrid nanofluid as a cooling fluid is 636.5 W, 655.5W, 669.7 W, respectively. Exergy production and usable heat gain supplied by PTC, including water, 0.25% MWCNT/0.25% Al_2O_3-water, and 1.5% MWCNT/1.5% Al_2O_3-water hybrid nanofluid, all follow the trend of solar radiation. The highest readings are recorded at 1:40 p.m. on January 13, 1:50 p.m. on April 30, 1:30:00 p.m. on July 14, and 1:40:00 p.m. on October 7. It should be noticed that these times coincide with the peak values of the direct solar radiation absorbed by the solar PTC. When the 1.5% MWCNT/1.5% Al_2O_3-water hybrid nanofluid is regarded as a cooling fluid, the maximum exergy production and usable is achieved. Increasing

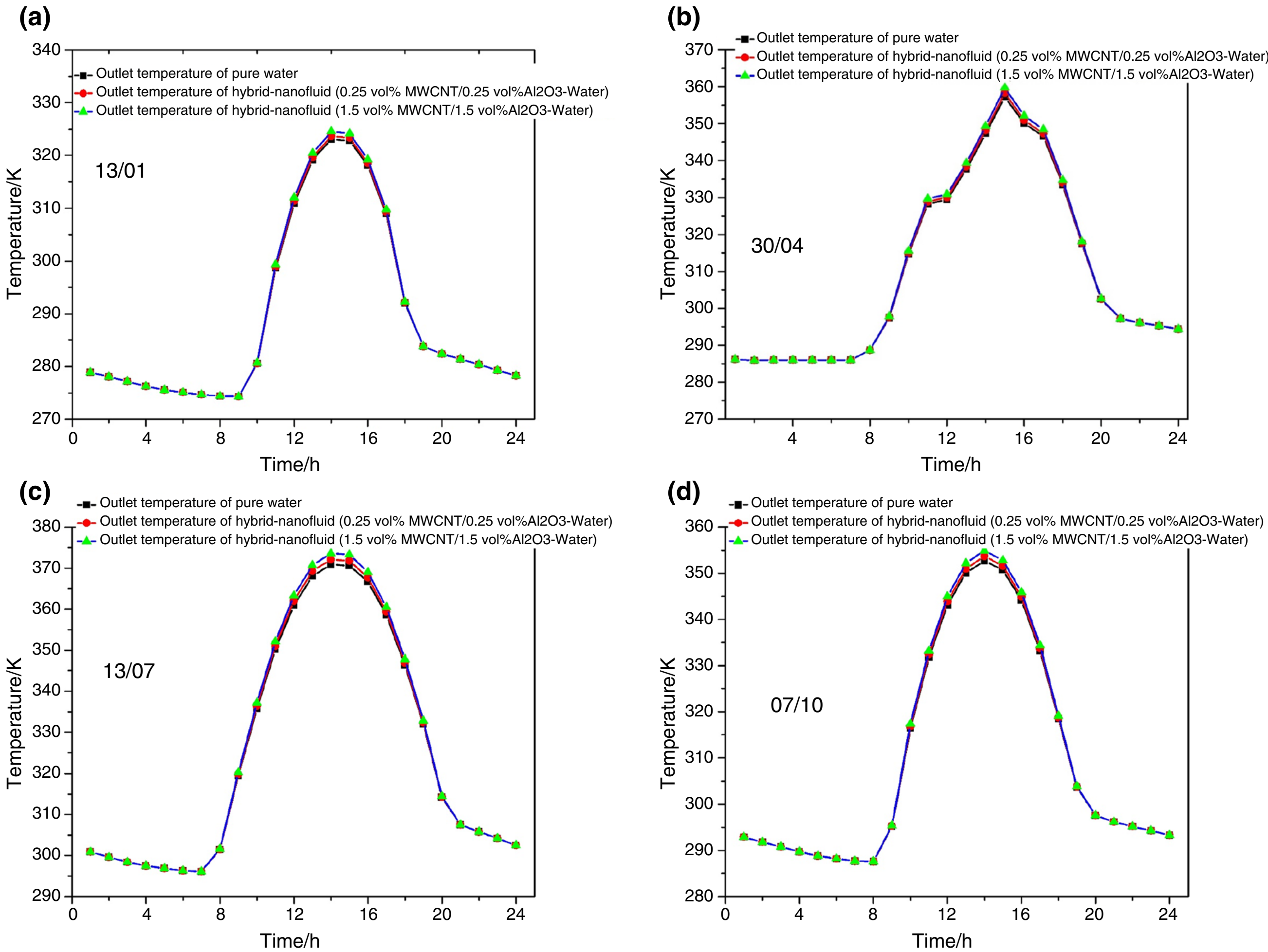

Fig. 11 Outlet fluid temperature for typical days (January 13, April 30, July 13, and October 7) under Ouarzazate climatic condition

the convective heat transfers between the cooling fluid and the absorber tube wall decreases their temperature gradient, resulting in a higher outlet fluid temperature. As a result, higher exergy production and usable heat gain are supplied by PTC.

Thermal and exergy efficiencies

The thermal and exergy efficiencies utilizing water, hybrid nanofluid provided by 0.25% MWCNT/0.25% Al_2O_3-water, and 1.5% MWCNT/1.5% Al_2O_3-water are illustrated in Figs. 14, 15 for typical days (January 13, April 30, July 13, and October 7) under Ouarzazate climatic conditions.

The maximal exergy efficiency obtained by PTC utilizing water, 0.25% MWCNT/0.25% Al_2O_3-water, and 1.5% MWCNT/1.5% Al_2O_3-water hybrid nanofluid as a cooling fluid on a selected overcast day (13/01) in the Ouarzazate area is 9.204%, 9.442%, and 9.642%, respectively. The maximal exergy efficiency obtained by PTC utilizing water, 0.25% MWCNT/0.25% Al_2O_3-water, and 1.5% MWCNT/1.5% Al_2O_3-water hybrid nanofluid as a cooling fluid on a selected summer day (13/07) in the Ouarzazate area is 12.59%, 13%, and 13.29%, respectively. The maximal exergy efficiency obtained by PTC utilizing water, 0.25% MWCNT/0.25% Al_2O_3 Al_2O_3-water, and 1.5% MWCNT/1.5% Al_2O_3-water hybrid nanofluid as a cooling fluid on a selected autumn day (07/10) in the Ouarzazate area is 11.36%, 11.7%, and 11.96%, respectively. The greatest exergy efficiency is attained when the 1.5% MWCNT/1.5% Al_2O_3-water hybrid nanofluid is used as a cooling fluid, increasing the convective heat transfers between the cooling fluid and the absorber

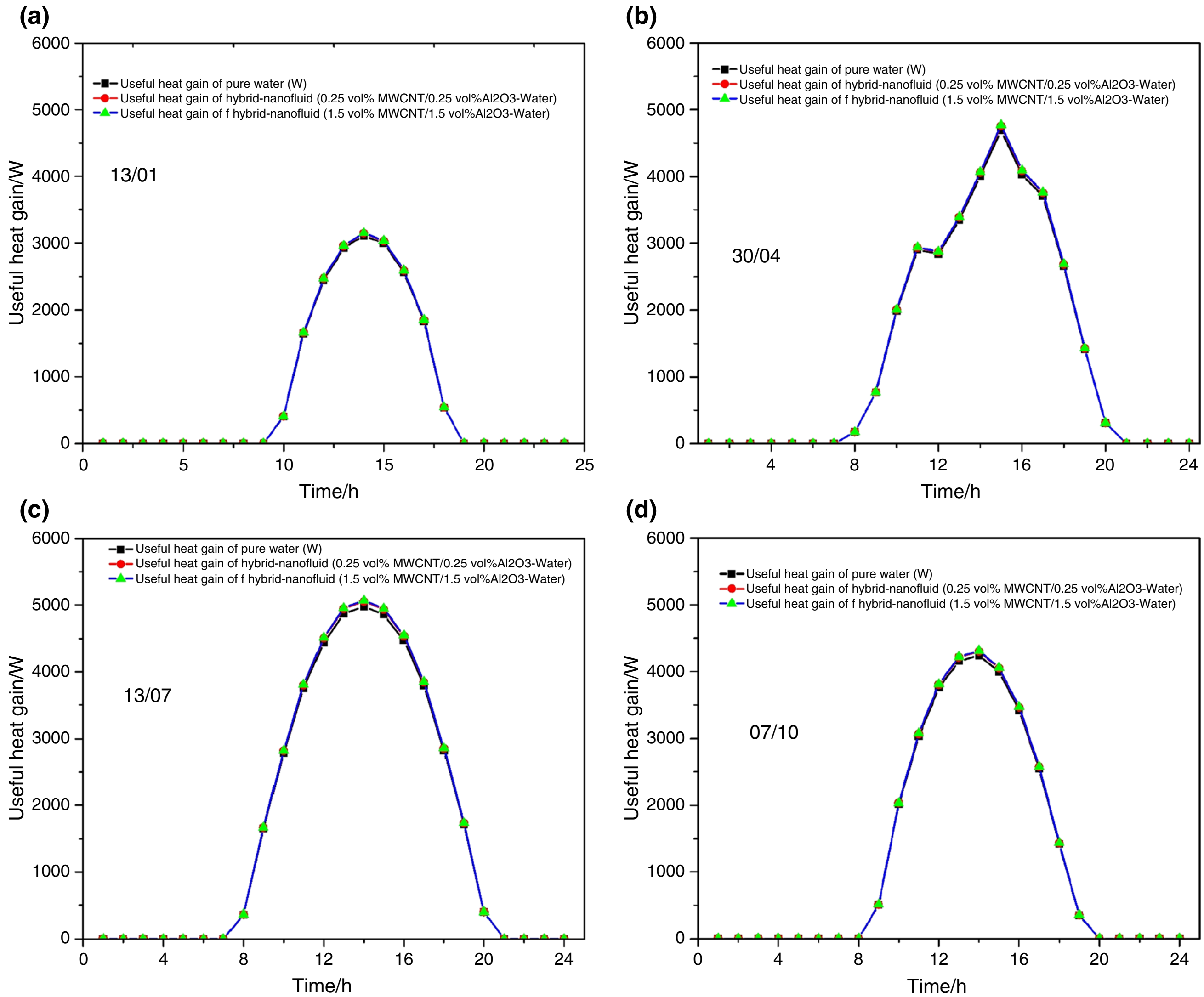

Fig. 12 Useful heat gain for typical days (January 13, April 30, July 13, and October 7) under Ouarzazate climatic conditions

tube wall, resulting in a higher output fluid temperature. As a consequence, PTC provides increased exergy efficiency.

Overall summary

Table 3 present a detailed comparison between the PTC with water, PTC with hybrid nanofluid (0.25% MWCNT/0.25% Al_2O_3-water), PTC with hybrid nanofluid (1.5% MWCNT/1.5% Al_2O_3-water) from the output fluid temperature, usable heat and exergy powers viewpoints under hot desert climate climatic conditions. The PTC's maximum thermal power output increased by 1.8% using a hybrid nanofluid (1.50% MWCNT/1.50% Al_2O_3-water). However, it can be improved by optimizing design parameters such as mass flow rate, inlet water temperature, nanoparticle concentration, size, and diameters. Their practical execution faces a variety of obstacles and limits, which are examined in depth in details in the following section.

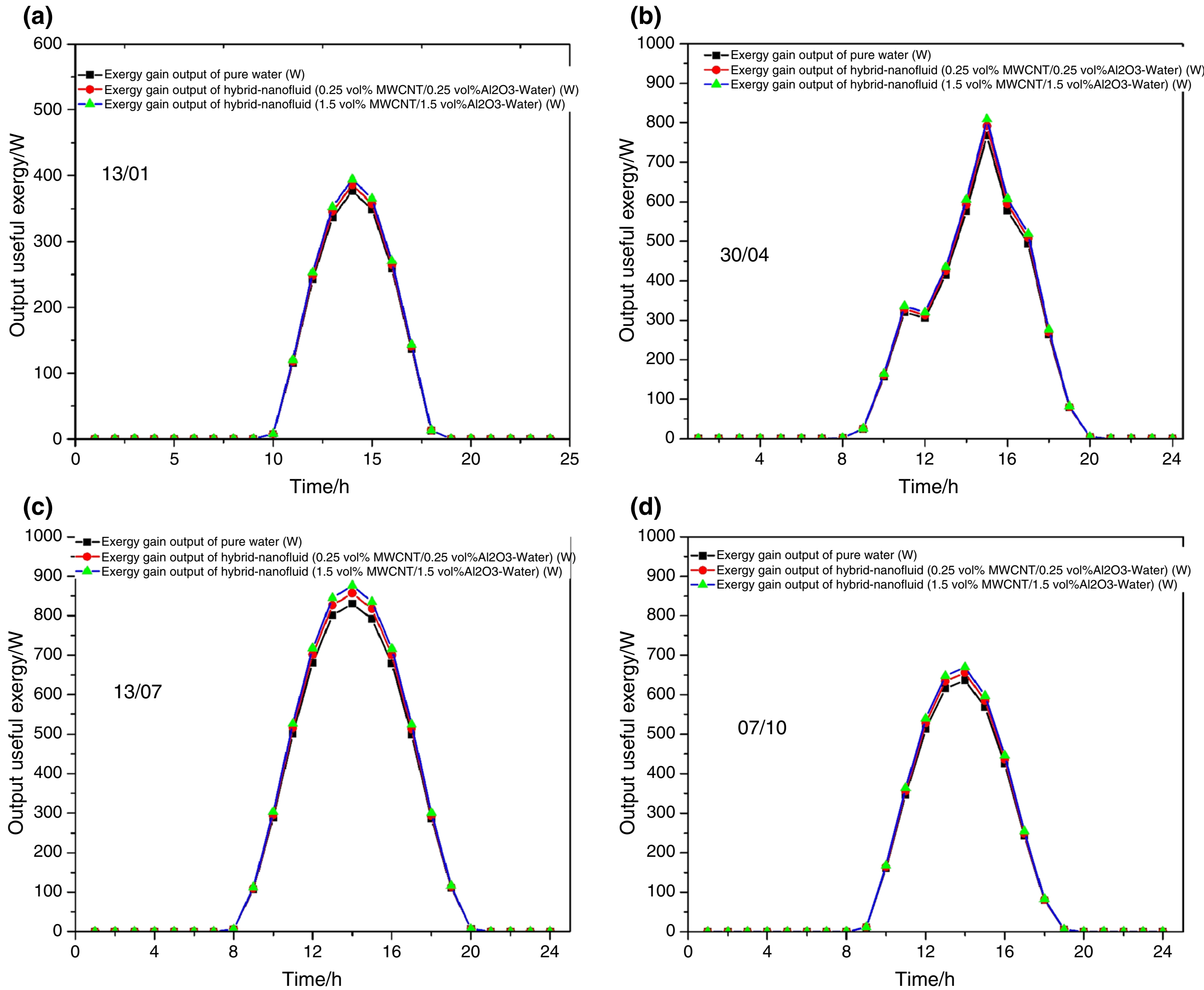

Fig. 13 Exergy output for typical days (January 13, April 30, July 13, and October 7) under Ouarzazate climatic conditions

Table 2 Design conditions of the proposed system

PTC input parameters [66, 67]		
Length	3.6	m
Width	1.22	m
Diameter of inner of the glazing	0.057	m
Diameter of outer of the glazing	0.06	m
Diameter of inner of the pipe	0.0158	m
Diameter of outer of the pipe	0.0178	m
Absorptance of the glazing	0.02	–
transmittance of the glazing	0.9	–
Emittance of the glazing	0.86	–
Mass flow rate	1	G.P.M
Intercept factor	0.48	–

Practical limitations and challenges of the use of the hybrid nanofluid in the PTC

The use of hybrid nanofluids as the working fluid in a PTC has only been tested and studied numerically. Only a few experimental efforts have been stated to address the evaluation and enhancement of the PTC over one day employing hybrid nanofluids as a working fluid. To assess the viability of commercial-scale hybrid nanofluid-based solar systems, conducting experimental long-term, feasible studies in terms of energy, exergy and economic performance is essential. In summary, whereas the hybrid nanofluids offer potential advantages for PTC collectors, using MWCNT/Al_2O_3-water as a heat transfer can boost efficiency and

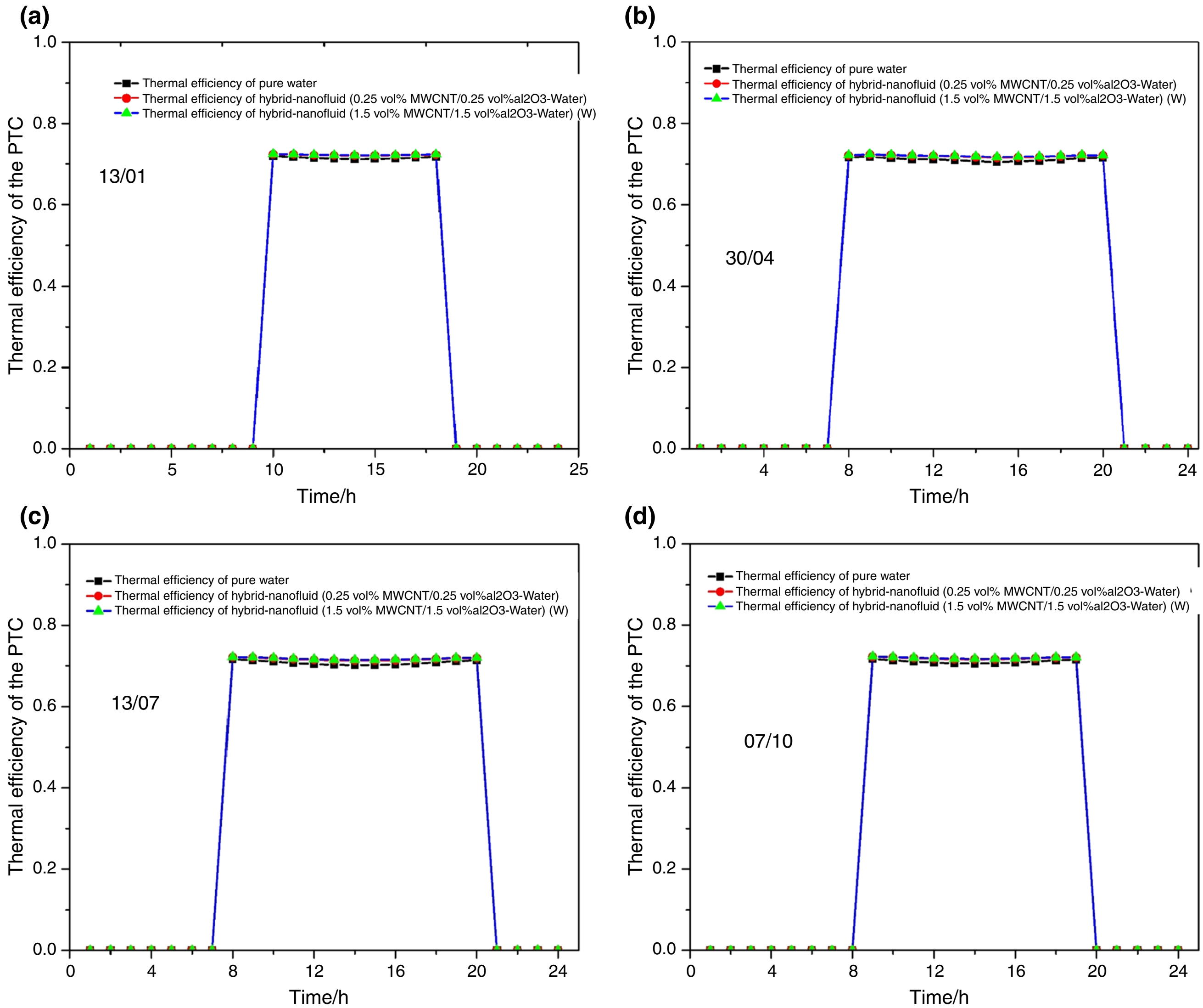

Fig. 14 Thermal efficiency for typical days (January 13, April 30, July 13, and October 7) under Ouarzazate climatic conditions

exergy performances by 1, 87% and 5.5%, respectively, compared to the base fluid. However, their practical implementation faces several difficulties and constraints (such as instability and high pumping power) discussed below that must be understood, solved and improved, focused on realizing their practical potential.

Instability Nanofluids are more than just a mixture of solid particles and fluid. Because of their high surface activity, nanoparticles tend to clump together. The agglomeration process generates particle sedimentation and duct sealing, reducing the nanofluids' suitable physical properties. As a result, nanofluid stability must be carefully evaluated. The concentration of nanoparticles, dispersing agents, viscosity, pH quantity, type of nanoparticles, the diameter of nanoparticles, and ultrasonication time are the most important characteristics determining the stability of nanofluids. Developing a stable nanofluid is required for optimizing nanofluid aspects. Nanoparticle aggregation and agglomeration increase the deposition probability, leading to decreased stability. Several approaches, such as pH adjustment of suspension, enhancement of surface activators, and use of ultrasonic vibrators, should be examined in the future to avoid nanoparticle aggregation and establish a stable combination.

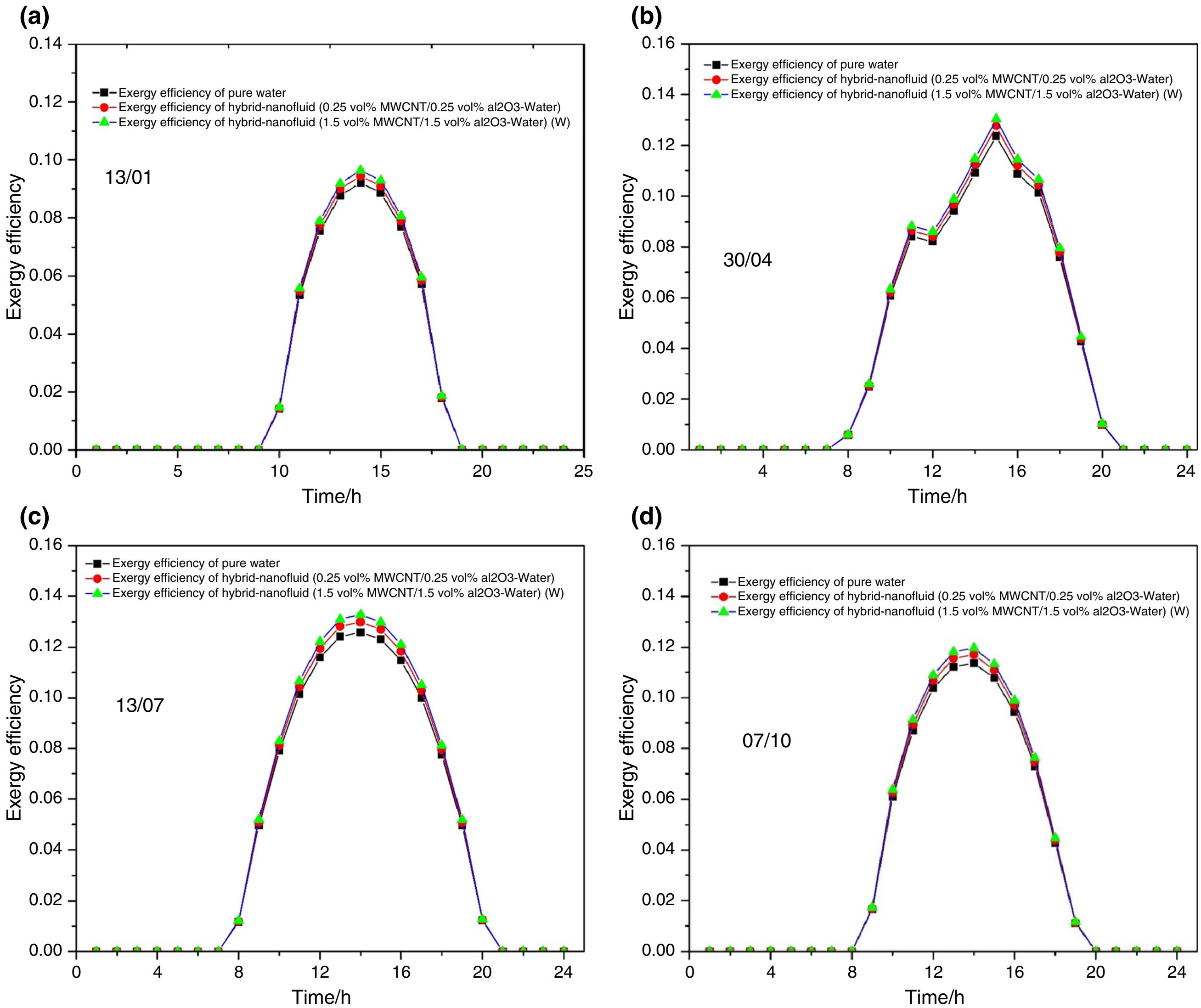

Fig. 15 The exergy efficiency for typical days (January 13, April 30, July 13, and October 7) under Ouarzazate climatic conditions

High pumping power requirements A critical issue with hybrid nanofluids is the unavoidable increase in friction factor. Because of the high friction factor, significant pumping power is required, preventing the benefits of hybrid nanofluids' enhanced heat transfer abilities from being achieved. The viscosity of the nanofluids increases when the concentration of the nanoparticles increases, leading to an increase in the friction factor. The viscosity is a resistive characteristic that generates shear stress against the force applied to the nanofluid. Viscosity is the driver of momentum transfer between nanofluid layers, and it appears when the layers move. Intermolecular forces are responsible for this. The presence of nanomaterials in the base fluid increases intermolecular forces, resulting in increased viscosity. Surfactants can reduce nanofluids' viscosity by negatively charging the nanoparticles, which causes them to repel each other and increase the number of collisions between the particles.

Table 3 Major findings from this study

PTC with water	PTC with hybrid nanofluid (0.25% MWCNT/0.25% Al_2O_3-water)	PTC with hybrid nanofluid (1.5% MWCNT/1.5% Al_2O_3-water)	Major findings
Outlet cooling temperature			
Winter day (13/01)			
1.3 °C to 50.1 °C	1.3 °C to 50.7	1.3 °C to 51.6 °C	Maximum outlet cooling temperatures for the PTC with a hybrid nanofluid (0.25% MWCNT/0.25% Al_2O_3-water) and the PTC with a hybrid nanofluid (1.50% MWCNT/1.50% Al_2O_3-water) are 1,197% and 2,994% higher than for the PTC with water as the cooling fluid, respectively, on a winter day
Spring day (30/04)			
13 °C to 84.2 °C	13 °C to 85.3 °C	13 °C to 86.7 °C	Maximum outlet cooling temperatures for the PTC with a hybrid nanofluid (0.25% MWCNT/0.25% Al_2O_3-water) and the PTC with a hybrid nanofluid (1.50% MWCNT/1.50% Al_2O_3-water) are 1,3064% and 2,9691% higher than for the PTC with water as the cooling fluid, respectively, on a springer day
Summer day (13/07)			
23.1 °C to 97.6 °C	23.1 °C to 99.1 °C	23.1 °C to 100.6 °C	Maximum outlet cooling temperatures for the PTC with a hybrid nanofluid (0.25% MWCNT/0.25% Al_2O_3-water) and the PTC with a hybrid nanofluid (1.50% MWCNT/1.50% Al_2O_3-water) are 1,5368% and 3,0737% higher than for the PTC with water as the cooling fluid, respectively, on a summer day
Autumn day (7 October)			
14.6 °C to 79.7 °C	14.6 °C to 80.7 °C	14.6 °C to 81.9 °C	Maximum outlet cooling temperatures for the PTC with a hybrid nanofluid (0.25% MWCNT/0.25% Al_2O_3-water) and the PTC with a hybrid nanofluid (1.50% MWCNT/1.50% Al_2O_3-water) are 1,2547% and 2,76035% higher than for the PTC with water as the cooling fluid, respectively, on an autumn day
Thermal power generated			
Winter day (13/01)			
3112W	3149W	3154W	Maximum thermal power generated by the PTC with a hybrid nanofluid (0.25% MWCNT/0.25% Al_2O_3-water) and by the PTC with a hybrid nanofluid (1.50% MWCNT/1.50% Al_2O_3-water) are 1,1889% and 1,34961% higher than by the PTC with water as the cooling fluid, respectively, on an winter day
Spring day (30/04)			
4689W	4760W	4772 W	Maximum thermal power generated by the PTC with a hybrid nanofluid (0.25% MWCNT/0.25% Al_2O_3-water) and by the PTC with a hybrid nanofluid (1.50% MWCNT/1.50% Al_2O_3-water) are 1,51418% and 1,7701% higher than by the PTC with water as the cooling fluid, respectively, on an springer day
Summer day (13/07)			
4973W	5052W	5066 W	Maximum thermal power generated by the PTC with a hybrid nanofluid (0.25% MWCNT/0.25% Al_2O_3-water) and by the PTC with a hybrid nanofluid (1.50% MWCNT/1.50% Al_2O_3-water) are 1,58857% and 1,87,009% higher than by the PTC with water as the cooling fluid, respectively, on an summer day

Table 3 (continued)

PTC with water	PTC with hybrid nanofluid (0.25% MWCNT/0.25% Al_2O_3-water)	PTC with hybrid nanofluid (1.5% MWCNT/1.5% Al_2O_3-water)	Major findings
Autumn day (7 October)			
4242 W	4302W	4312W	Maximum thermal power generated by the PTC with a hybrid nanofluid (0.25% MWCNT/0.25% Al_2O_3-water) and by the PTC with a hybrid nanofluid (1.50% MWCNT/1.50% Al_2O_3-water) are 1,414% and 1,65% higher than by the PTC with water as the cooling fluid, respectively, on an autumn day
Exergy power generated			
Winter day (13/01)			
376.3 W	386.1W	394.2W	Maximum exergy power generated by the PTC with a hybrid nanofluid (0.25% MWCNT/0.25% Al_2O_3-water) and by the PTC with a hybrid nanofluid (1.50% MWCNT/1.50% Al_2O_3-water) are 2,6043% and 4,7568% higher than by the PTC with water as the cooling fluid, respectively, on an winter day
Spring day (30/04)			
767.7W	791.7W	808.8 W	Maximum exergy power generated by the PTC with a hybrid nanofluid (0.25% MWCNT/0.25% Al_2O_3-water) and by the PTC with a hybrid nanofluid (1.50% MWCNT/1.50% Al_2O_3-water) are 3,9% and 5,35365% higher than by the PTC with water as the cooling fluid, respectively, on an springer day
Summer day (13/07)			
829.9 W	857W	876W	Maximum exergy power generated by the PTC with a hybrid nanofluid (0.25% MWCNT/0.25% Al_2O_3-water) and by the PTC with a hybrid nanofluid (1.50% MWCNT/1.50% Al_2O_3-water) are 3,2654% and 5,5548% higher than by the PTC with water as the cooling fluid, respectively, on an summer day
Autumn day (7 October)			
636.5 W	655.5W	669.7 W	Maximum exergy power generated by the PTC with a hybrid nanofluid (0.25% MWCNT/0.25% Al_2O_3-water) and by the PTC with a hybrid nanofluid (1.50% MWCNT/1.50% Al_2O_3-water) are 2,98% and 5,21% higher than by the PTC with water as the cooling fluid, respectively, on an autumn day

Conclusions

Innovative heat transfer fluids called hybrid nanofluids combine a base fluid with solid nanometer-sized particles (nanoparticles) to greatly improve the fluid's thermal characteristics and the system's thermal performance. In this study, a hybrid nanofluid was employed as the working fluid for the PTC. In a subtropical desert with mild winters and sweltering, sunny summers, this research presents a complete thermo-mathematical numerical analysis of PTC collectors using multi-wall carbon nanotube-aluminium oxide (MWCNT/ Al_2O_3) hybrid nanofluids. An Engineering Equation Solver is used to calculate the effects of temperature changes on the solar collector's thermodynamic (energy, exergy) performance in a hot desert environment (EES). After first comparing the numerical model to previously published experimental data, a satisfactory level of agreement was found. The results show that a higher concentration of nanoparticles may improve the PTC collector's functionality. PTC collector output temperature, energy, and exergy maximums are attained when the hybrid nanofluid of 1.5% MWCNT/1.5% Al_2O_3-water is considered a cooling fluid. In hot weather, the PTC performs well, but in cold weather, it struggles. Energy output and exergy output from a PTC operating with a 1.5% MWCNT/1.5% Al_2O_3-water hybrid nanofluid on a summer day are 5066 W and 876 W, respectively. 1,58,857% and 1,87,009 enhancements in the maximum thermal power produced by the PTC using a hybrid nanofluid (0.25% MWCNT/0.25% Al_2O_3-water), and using hybrid nanofluid (1.50% MWCNT/1.50% Al_2O_3-water) for the summer day, whereas that for the winter day are 1,1889% and 1,34,961%, respectively, in comparison with the typical PTC system using water as the cooling fluid.

More research is needed in the future to perform long-term, practical investigations on the energy, exergy, and economic performances of the PTC employing a hybrid nanofluid as a cooling fluid.

References

1. Rejeb O, Radwan A, Abo-Zahhad EM, Ghenai C, Serageldin AA, Ahmed M, et al. Numerical analysis of passive cooled ultra-high concentrator photovoltaic cell using optimal heat spreader design. Case Stud Therm Eng. 2020. https://doi.org/10.1016/j.csite.2020.100757.
2. Ghenai C, Ahmad FF, Rejeb O, Hamid AK. Sensitivity analysis of design parameters and power gain correlations of bi-facial solar PV system using response surface methodology. Sol Energy. 2021;223:44–53. https://doi.org/10.1016/j.solener.2021.05.024.
3. Rejeb O, Alirahmi SM, Assareh E, El Haj AM, Jemni A, Bettayeb M, et al. Innovative integrated solar powered polygeneration system for green Hydrogen, Oxygen, electricity and heat production. Energy Convers Manag. 2022;269:116073. https://doi.org/10.1016/j.enconman.2022.116073.
4. Ghenai C, Ahmad FF, Rejeb O, Bettayeb M. Artificial neural networks for power output forecasting from bifacial solar PV system with enhanced building roof surface Albedo. J Build Eng. 2022;56:104799. https://doi.org/10.1016/j.jobe.2022.104799.
5. Parker W, Odukomaiya A, Thornton J, Woods J. The cost savings potential of controlling solar thermal collectors with storage for time-of-use electricity rates. Sol Energy. 2023;249:684–93. https://doi.org/10.1016/j.solener.2022.12.004.
6. Chai S, Yao J, Liang J-D, Chiang Y-C, Zhao Y, Chen S-L, et al. Heat transfer analysis and thermal performance investigation on an evacuated tube solar collector with inner concentrating by reflective coating. Sol Energy. 2021;220:175–86. https://doi.org/10.1016/j.solener.2021.03.048.
7. Rodríguez-Muñoz JM, Bove I, Alonso-Suárez R. Novel incident angle modifier model for quasi-dynamic testing of flat plate solar thermal collectors. Sol Energy. 2021;224:112–24. https://doi.org/10.1016/j.solener.2021.05.026.
8. Jiang Y, Zhang H, Zhao R, Liu Z, Wang Y, You S, et al. Thermal and optical performance analysis of triangular solar air collectors and regional applicability in China. Sol Energy. 2023;249:288–300. https://doi.org/10.1016/j.solener.2022.11.010.
9. Sivakumar M, Mahalingam S, Mohanraj M. Energy, financial and environmental impact analysis of solar thermal heat pump systems using a direct expansion packed bed evaporator-collector. Sol Energy. 2022;232:154–68. https://doi.org/10.1016/j.solener.2021.12.059.
10. Chand S, Chand P, Kumar GH. Thermal performance enhancement of solar air heater using louvered fins collector. Sol Energy. 2022;239:10–24. https://doi.org/10.1016/j.solener.2022.04.046.
11. Perini S, Tonnellier X, King P, Sansom C. Theoretical and experimental analysis of an innovative dual-axis tracking linear Fresnel lenses concentrated solar thermal collector. Sol Energy. 2017;153:679–90. https://doi.org/10.1016/j.solener.2017.06.010.
12. Abbas R, Montes MJ, Rovira A, Martínez-Val JM. Parabolic trough collector or linear Fresnel collector? A comparison of optical features including thermal quality based on commercial solutions. Sol Energy. 2016;124:198–215. https://doi.org/10.1016/j.solener.2015.11.039.
13. Zhou L, Li X, Zhao Y, Dai Y. Performance assessment of a single/double hybrid effect absorption cooling system driven by linear Fresnel solar collectors with latent thermal storage. Sol Energy. 2017;151:82–94. https://doi.org/10.1016/j.solener.2017.05.031.
14. Moghimi MA, Craig KJ, Meyer JP. Simulation-based optimisation of a linear Fresnel collector mirror field and receiver for optical, thermal and economic performance. Sol Energy. 2017;153:655–78. https://doi.org/10.1016/j.solener.2017.06.001.
15. Dhaked DK, Birla D. Modeling and control of a solar-thermal dish-stirling coupled PMDC generator and battery based DC microgrid in the framework of the ENERGY NEXUS. Energy Nexus. 2022;5:100048. https://doi.org/10.1016/j.nexus.2022.100048.
16. Li X, Li R, Hu L, Zhu S, Zhang Y, Cui X, et al. Performance analysis of a dish solar thermal power system with lunar regolith heat storage for continuous energy supply of lunar base. Energy. 2023;263:126139. https://doi.org/10.1016/j.energy.2022.126139.
17. Bitam EW, Demagh Y, Hachicha AA, Benmoussa H, Kabar Y. Numerical investigation of a novel sinusoidal tube receiver for parabolic trough technology. Appl Energy. 2018;218:494–510. https://doi.org/10.1016/j.apenergy.2018.02.177.
18. Hachicha AA, Yousef BAA, Said Z, Rodríguez I. A review study on the modeling of high-temperature solar thermal collector systems. Renew Sustain Energy Rev. 2019;112:280–98. https://doi.org/10.1016/j.rser.2019.05.056.
19. Hachicha AA, Rodríguez I, Ghenai C. Thermo-hydraulic analysis and numerical simulation of a parabolic trough solar collector for direct steam generation. Appl Energy. 2018;214:152–65. https://doi.org/10.1016/j.apenergy.2018.01.054.
20. Hachicha AA, Rodríguez I, Capdevila R, Oliva A. Heat transfer analysis and numerical simulation of a parabolic trough solar collector. Appl Energy. 2013;111:581–92. https://doi.org/10.1016/j.apenergy.2013.04.067.
21. Hachicha AA, Rodríguez I, Castro J, Oliva A. Numerical simulation of wind flow around a parabolic trough solar collector. Appl Energy. 2013;107:426–37. https://doi.org/10.1016/j.apenergy.2013.02.014.
22. Immonen J, Mohammadi K, Powell KM. Simulating a solar parabolic trough collector plant used for industrial process heat using an optimized operating scheme that utilizes flexible heat integration. Sol Energy. 2022;236:756–71. https://doi.org/10.1016/j.solener.2022.03.044.
23. Ben Othman F, Eddhibi F, Bel Hadj Ali A, Fadhel A, Bayer Ö, Tarı İ, et al. Investigation of olive mill sludge treatment using a parabolic trough solar collector. Sol Energy. 2022;232:344–61. https://doi.org/10.1016/j.solener.2022.01.008.
24. Pandey M, Padhi BN, Mishra I. Numerical simulation of solar parabolic trough collector with viscous dissipation in slits of arc-plug insertion. Sol Energy. 2021;230:810–24. https://doi.org/10.1016/j.solener.2021.11.008.
25. Jinshah BS, Balasubramanian KR. Thermo-mathematical model for parabolic trough collector using a complete radiation heat transfer model – A new approach. Sol Energy. 2020;197:58–72. https://doi.org/10.1016/j.solener.2019.12.068.
26. Madiouli J, Lashin A, Shigidi I, Badruddin IA, Kessentini A. Experimental study and evaluation of single slope solar still combined with flat plate collector, parabolic trough and packed bed.

Sol Energy. 2020;196:358–66. https://doi.org/10.1016/j.solener.2019.12.027.

27. Yahi F, Belhamel M, Bouzeffour F, Sari O. Structured dynamic modeling and simulation of parabolic trough solar collector using bond graph approach. Sol Energy. 2020;196:27–38. https://doi.org/10.1016/j.solener.2019.11.065.
28. Okonkwo EC, Essien EA, Akhayere E, Abid M, Kavaz D, Ratlamwala TAH. Thermal performance analysis of a parabolic trough collector using water-based green-synthesized nanofluids. Sol Energy. 2018;170:658–70. https://doi.org/10.1016/j.solener.2018.06.012.
29. Fathy M, Hassan H, Salem AM. Experimental study on the effect of coupling parabolic trough collector with double slope solar still on its performance. Sol Energy. 2018;163:54–61. https://doi.org/10.1016/j.solener.2018.01.043.
30. Bellos E, Tzivanidis C, Belessiotis V. Daily performance of parabolic trough solar collectors. Sol Energy. 2017;158:663–78. https://doi.org/10.1016/j.solener.2017.10.038.
31. Sallaberry F, Valenzuela L, Palacin LG. On-site parabolic-trough collector testing in solar thermal power plants: Experimental validation of a new approach developed for the IEC 62862–3-2 standard. Sol Energy. 2017;155:398–409. https://doi.org/10.1016/j.solener.2017.06.045.
32. Farooq M, Farhan M, Ahmad G, ul Tahir ZR, Usman M, Sultan M, et al. Thermal performance enhancement of nanofluids based parabolic trough solar collector (NPTSC) for sustainable environment. Alexandria Eng J. 2022;61:8943–53. https://doi.org/10.1016/j.aej.2022.02.029.
33. Chafie M, Ben Aissa MF, Guizani A. Energetic end exergetic performance of a parabolic trough collector receiver: an experimental study. J Clean Prod. 2018;171:285–96. https://doi.org/10.1016/j.jclepro.2017.10.012.
34. Gomna A, N'Tsoukpoe KE, Le Pierrès N, Coulibaly Y. Review of vegetable oils behaviour at high temperature for solar plants: Stability, properties and current applications. Sol Energy Mater Sol Cells. 2019;200:109956. https://doi.org/10.1016/j.solmat.2019.109956.
35. Giaconia A, Iaquaniello G, Metwally AA, Caputo G, Balog I. Experimental demonstration and analysis of a CSP plant with molten salt heat transfer fluid in parabolic troughs. Sol Energy. 2020;211:622–32. https://doi.org/10.1016/j.solener.2020.09.091.
36. Fredriksson J, Eickhoff M, Giese L, Herzog M. A comparison and evaluation of innovative parabolic trough collector concepts for large-scale application. Sol Energy. 2021;215:266–310. https://doi.org/10.1016/j.solener.2020.12.017.
37. Martínez-Merino P, Alcántara R, Gómez-Larrán P, Carrillo-Berdugo I, Navas J. MoS2-based nanofluids as heat transfer fluid in parabolic trough collector technology. Renew Energy. 2022;188:721–30. https://doi.org/10.1016/j.renene.2022.02.069.
38. Malekan M, Khosravi A, Syri S. Heat transfer modeling of a parabolic trough solar collector with working fluid of Fe3O4 and CuO/Therminol 66 nanofluids under magnetic field. Appl Therm Eng. 2019;163:114435. https://doi.org/10.1016/j.applthermaleng.2019.114435.
39. Chavez Panduro EA, Finotti F, Largiller G, Lervåg KY. A review of the use of nanofluids as heat-transfer fluids in parabolic-trough collectors. Appl Therm Eng. 2022;211:118346. https://doi.org/10.1016/j.applthermaleng.2022.118346.
40. do Carmo Zidan D, Brasil Maia C, Reza SM. Performance evaluation of various nanofluids for parabolic trough collectors. Sustain Energy Technol Assessments. 2022;50:101865. https://doi.org/10.1016/j.seta.2021.101865.
41. Abidi A, El-Shafay AS, Degani M, Guedri K, Mohammad Sajadi S, Sharifpur M. Improving the thermal-hydraulic performance of parabolic solar collectors using absorber tubes equipped with perforated twisted tape containing nanofluid. Sustain Energy Technol Assessments. 2022;52:102099. https://doi.org/10.1016/j.seta.2022.102099.
42. Tiwari AK, Kumar V, Said Z, Paliwal HK. A review on the application of hybrid nanofluids for parabolic trough collector: Recent progress and outlook. J Clean Prod. 2021;292:126031. https://doi.org/10.1016/j.jclepro.2021.126031.
43. Bellos E, Said Z, Tzivanidis C. The use of nanofluids in solar concentrating technologies: a comprehensive review. J Clean Prod. 2018;196:84–99. https://doi.org/10.1016/j.jclepro.2018.06.048.
44. Bellos E, Tzivanidis C, Antonopoulos KA, Gkinis G. Thermal enhancement of solar parabolic trough collectors by using nanofluids and converging-diverging absorber tube. Renew Energy. 2016;94:213–22. https://doi.org/10.1016/j.renene.2016.03.062.
45. Kumar K, Kumar R, Bharj RS, Said Z. Effect of arc corrugation initiation on the thermo-hydraulic performance and entropy generation of the corrugated tube. Int Commun Heat Mass Transf. 2022;138:106335. https://doi.org/10.1016/j.icheatmasstransfer.2022.106335.
46. Bellos E, Tzivanidis C. Investigation of a star flow insert in a parabolic trough solar collector. Appl Energy. 2018;224:86–102. https://doi.org/10.1016/j.apenergy.2018.04.099.
47. Bellos E, Tzivanidis C, Tsimpoukis D. Multi-criteria evaluation of parabolic trough collector with internally finned absorbers. Appl Energy. 2017;205:540–61. https://doi.org/10.1016/j.apenergy.2017.07.141.
48. Zhu X, Zhu L, Zhao J. Wavy-tape insert designed for managing highly concentrated solar energy on absorber tube of parabolic trough receiver. Energy. 2017;141:1146–55. https://doi.org/10.1016/j.energy.2017.10.010.
49. Jaramillo OA, Borunda M, Velazquez-Lucho KM, Robles M. Parabolic trough solar collector for low enthalpy processes: an analysis of the efficiency enhancement by using twisted tape inserts. Renew Energy. 2016;93:125–41. https://doi.org/10.1016/j.renene.2016.02.046.
50. Yılmaz İH, Mwesigye A, Göksu TT. Enhancing the overall thermal performance of a large aperture parabolic trough solar collector using wire coil inserts. Sustain Energy Technol Assessments. 2020;39:100696. https://doi.org/10.1016/j.seta.2020.100696.
51. Hachicha AA, Said Z, Rahman SMA, Al-Sarairah E. On the thermal and thermodynamic analysis of parabolic trough collector technology using industrial-grade MWCNT based nanofluid. Renew Energy. 2020;161:1303–17. https://doi.org/10.1016/j.renene.2020.07.096.
52. Bellos E, Tzivanidis C. Thermal analysis of parabolic trough collector operating with mono and hybrid nanofluids. Sustain Energy Technol Assessments. 2018;26:105–15. https://doi.org/10.1016/j.seta.2017.10.005.
53. Ehyaei MA, Ahmadi A, Assad MEH, Hachicha AA, Said Z. Energy, exergy and economic analyses for the selection of working fluid and metal oxide nanofluids in a parabolic trough collector. Sol Energy. 2019;187:175–84. https://doi.org/10.1016/j.solener.2019.05.046.
54. Kazemian A, Salari A, Ma T, Lu H. Application of hybrid nanofluids in a novel combined photovoltaic/thermal and solar collector system. Sol Energy. 2022;239:102–16. https://doi.org/10.1016/j.solener.2022.04.016.
55. Kalogirou SA. A detailed thermal model of a parabolic trough collector receiver. Energy. 2012;48:298–306. https://doi.org/10.1016/j.energy.2012.06.023.
56. Allouhi A, Benzakour Amine M, Saidur R, Kousksou T, Jamil A. Energy and exergy analyses of a parabolic trough collector operated with nanofluids for medium and high temperature applications. Energy Convers Manag. 2018;155:201–17. https://doi.org/10.1016/j.enconman.2017.10.059.

57. Allouhi A, Benzakour Amine M, Kousksou T, Jamil A, Lahrech K. Yearly performance of low-enthalpy parabolic trough collectors in MENA region according to different sun-tracking strategies. Appl Therm Eng. 2018;128:1404–19. https://doi.org/10.1016/j.applthermaleng.2017.09.099.
58. Lamrani B, Khouya A, Zeghmati B, Draoui A. Mathematical modeling and numerical simulation of a parabolic trough collector: a case study in thermal engineering. Therm Sci Eng Prog. 2018;8:47–54. https://doi.org/10.1016/j.tsep.2018.07.015.
59. Lamrani B, Khouya A, Draoui A. Thermal performance of a parabolic trough collector under different climatic zones in Morocco. AIP Conf Proc. 2018;2056:20007. https://doi.org/10.1063/1.5084980.
60. Lamrani B, Kuznik F, Draoui A. Thermal performance of a coupled solar parabolic trough collector latent heat storage unit for solar water heating in large buildings. Renew Energy. 2020;162:411–26. https://doi.org/10.1016/j.renene.2020.08.038.
61. Minea AA. Chapter 7 - Barriers and challenges in hybrid nanofluids development and implementation. In: Ali HM, editor. Hybrid nanofluids for convection heat transfer. Cambridge: Academic Press; 2020.
62. Hemmat Esfe M, Esfandeh S, Kamyab MH. Chapter 1 - History and introduction. In: Ali HM, editor. Hybrid nanofluids for convection heat transfer. Cambridge: Academic Press; 2020.
63. Jamil F, Ali HM. Chapter 6 - Applications of hybrid nanofluids in different fields. In: Ali HM, editor. Hybrid nanofluids for convection heat transfer. Cambridge: Academic Press; 2020.
64. Shah TR, Koten H, Ali HM. Chapter 5 - Performance effecting parameters of hybrid nanofluids. In: Ali HM, editor. Hybrid nanofluids for convection heat transfer. Cambridge: Academic Press; 2020.
65. Babar H, Sajid MU, Ali HM. Chapter 4 - Hybrid nanofluids as a heat transferring media. In: Ali HM, editor. Hybrid nanofluids for convection heat transfer. Cambridge: Academic Press; 2020.
66. Alfellag M. Modeling and exprimental investigation of parabolic trough solar collector. Embry-Riddle Aeronautical University – Daytona Beach. 2014
67. Mercan H. Chapter 3 - Thermophysical and rheological properties of hybrid nanofluids. In: Ali HM, editor. Hybrid nanofluids for convection heat transfer. Cambridge: Academic Press; 2020.
68. Afrand M, Ranjbarzadeh R. Chapter 2 - Hybrid nanofluids preparation method. In: Ali HM, editor. Hybrid nanofluids for convection heat transfer. Cambridge: Academic Press; 2020.
69. Eshgarf H, Kalbasi R, Maleki A, Shadloo MS, Karimipour A. A review on the properties, preparation, models and stability of hybrid nanofluids to optimize energy consumption. J Therm Anal Calorim. 2021;144:1959–83. https://doi.org/10.1007/s10973-020-09998-w.
70. Shah TR, Ali HM. Applications of hybrid nanofluids in solar energy, practical limitations and challenges: A critical review. Sol Energy. 2019;183:173–203. https://doi.org/10.1016/j.solener.2019.03.012.
71. Sajid MU, Ali HM. Thermal conductivity of hybrid nanofluids: a critical review. Int J Heat Mass Transf. 2018;126:211–34. https://doi.org/10.1016/j.ijheatmasstransfer.2018.05.021.
72. Babar H, Ali HM. Towards hybrid nanofluids: preparation, thermophysical properties, applications, and challenges. J Mol Liq. 2019;281:598–633. https://doi.org/10.1016/j.molliq.2019.02.102.